

AD-A220 175

NAVAL POSTGRADUATE SCHOOL Monterey, California



SDTIC
ELECTE
APR 5 1990
B
lt

THESIS

A RANGE-DEPENDENT ANALYSIS OF
ACOUSTIC TRANSMISSION ACROSS
A COLD FILAMENT IN THE
CALIFORNIA CURRENT

by

Lawrence M. Jendro

September 1989

Co-Advisor
Co-Advisor

Steven R. Ramp
Robert H. Bourke

Approved for public release;
distribution unlimited.

Unclassified

security classification of this page

REPORT DOCUMENTATION PAGE				
1a Report Security Classification Unclassified			1b Restrictive Markings	
2a Security Classification Authority			3 Distribution Availability of Report Approved for public release; distribution is unlimited.	
2b Declassification Downgrading Schedule				
4 Performing Organization Report Number(s)			5 Monitoring Organization Report Number(s)	
6a Name of Performing Organization Naval Postgraduate School		6b Office Symbol (if applicable) 52	7a Name of Monitoring Organization Naval Postgraduate School	
6c Address (city, state, and ZIP code) Monterey, CA 93943-5000			7b Address (city, state, and ZIP code) Monterey, CA 93943-5000	
8a Name of Funding Sponsoring Organization		8b Office Symbol (if applicable)	9 Procurement Instrument Identification Number	
8c Address (city, state, and ZIP code)			10 Source of Funding Numbers	
			Program Element No	Project No
			Task No	Work Unit Accession No
11 Title (include security classification) A RANGE-DEPENDENT ANALYSIS OF ACOUSTIC TRANSMISSION ACROSS A COLD FILAMENT IN THE CALIFORNIA CURRENT				
12 Personal Author S. Lawrence M. Jendro				
13a Type of Report Master's Thesis		13b Time Covered From To	14 Date of Report (year, month, day) September 1989	15 Page Count 73
16 Supplementary Notation The views expressed in this thesis are those of the author and do not reflect the official policy or position of the Department of Defense or the U.S. Government.				
17 Cross Codes			18 Subject Terms (continue on reverse if necessary and identify by block number)	
Field	Group	Subgroup	cold filament, acoustic propagation, predicted sonar range.	
19 Abstract (continue on reverse if necessary and identify by block number)				
<p>CTD data were taken in a area where satellite imagery had detected a cold water filament to frequently recur in the California Current System in order to determine the temporal and spatial variability of the hydrographic and velocity fields. Sound speed profiles were constructed from this data and predicted sonar ranges (PSRs) were computed for passive sonar using a range-dependent parabolic equation model. Analysis of model results applied to tactical scenarios showed the acoustic advantage between two adversaries to change as their positions relative to the front and to each other were changed. An investigation of the acoustic mechanisms involved in the variation of PSRs showed that small variations in surface temperature were enough to cause significant changes in PSRs. Changes in temperature of sufficient magnitude to effect PSRs were found also in SST imagery of cold filaments in other eastern boundary currents around the world.</p>				
20 Distribution Availability of Abstract <input checked="" type="checkbox"/> unclassified unlimited <input type="checkbox"/> same as report <input type="checkbox"/> DTIC users			21 Abstract Security Classification Unclassified	
22a Name of Responsible Individual Steven R. Ramp			22b Telephone (include Area code) (408) 646-3270	22c Office Symbol 68Ra

DD FORM 1473.84 MAR

83 APR edition may be used until exhausted
All other editions are obsolete

security classification of this page

Unclassified

Approved for public release; distribution is unlimited.

A Range-Dependent Analysis of
Acoustic Transmission Across
a Cold Filament in the
California Current

by

Lawrence M. Jendro
Lieutenant Commander, United States Navy
B.S., University of Washington, 1978

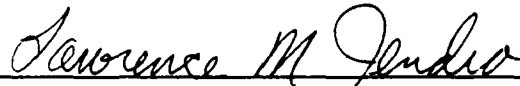
Submitted in partial fulfillment of the
requirements for the degree of

MASTER OF SCIENCE IN METEOROLOGY AND PHYSICAL
OCEANOGRAPHY

from the

NAVAL POSTGRADUATE SCHOOL
September 1989

Author:

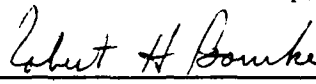


Lawrence M. Jendro

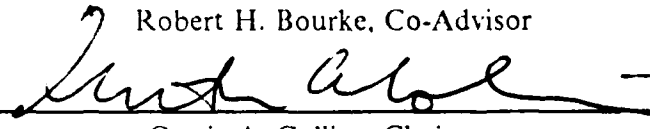
Approved by:



Steven R. Ramp, Co-Advisor



Robert H. Bourke, Co-Advisor



Curtis A. Collins, Chairman,
Department of Oceanography

ABSTRACT

CTD data were taken in a area where satellite imagery had detected a cold water filament to frequently recur in the California Current System in order to determine the temporal and spatial variability of the hydrographic and velocity fields. Sound speed profiles were constructed from this data and predicted sonar ranges (PSRs) were computed for passive sonar using a range-dependent parabolic equation model. Analysis of model results applied to tactical scenarios showed the acoustic advantage between two adversaries to change as their positions relative to the front and to each other were changed. An investigation of the acoustic mechanisms involved in the variation of PSRs showed that small variations in surface temperature were enough to cause significant changes in PSRs. Changes in temperature of sufficient magnitude to effect PSRs were found also in SST imagery of cold filaments in other eastern boundary currents around the world.

Accession For	
NTIS GRA&I	<input checked="checked" type="checkbox"/>
DTIC TAB	<input type="checkbox"/>
Unannounced	<input type="checkbox"/>
Justification	
By	
Distribution/	
Availability Codes	
Dist	Avail and/or Special
A-1	

TABLE OF CONTENTS

I. INTRODUCTION	1
II. DATA AND METHODOLOGY	4
A. DATA ACQUISITION	4
B. SOUND SPEED PROFILES	4
C. THE PARABOLIC EQUATION ACOUSTIC MODEL	5
D. PREDICTED SONAR RANGES	6
III. RESULTS	11
A. A. VERTICAL CROSS SECTIONS	11
B. ANALYSIS OF SOUND SPEED PROFILES	12
C. RESULTING PREDICTED SONAR RANGES	15
1. Variation of PSRs with frequency	16
2. Variation of PSRs with receiver depth	16
3. Variation of PSRs with mixed layer depth	16
4. Variation of PSRs with surface temperature	16
5. Variation in PSRs due to shallow SSP structure	16
6. Variations in PSRs showing acoustic asymmetry across the front	17
IV. DISCUSSION	44
A. OCEANOGRAPHY	44
B. ACOUSTICS	46
1. The Nature of the Front	46
2. The Effects of the Acoustic Front	48
3. The Tactical Significance of Variations in PSRs	49
4. Applicability to Other Eastern Boundary Regions	50
V. CONCLUSION	59
INITIAL DISTRIBUTION LIST	64

LIST OF TABLES

Table 1.	MIXED LAYER DEPTH AND LOW FREQUENCY CUTOFF AT EACH STATION.	19
Table 2.	PREDICTED SONAR RANGES FOR A SOURCE AT 5 M DEPTH, PROJECTING SOUTHWARD.	32
Table 3.	PREDICTED SONAR RANGES FOR A SOURCE AT 100 M DEPTH, PROJECTING SOUTHWARD.	33
Table 4.	PREDICTED SONAR RANGES FOR A SOURCE AT 5 M DEPTH, PROJECTING NORTHWARD.	34
Table 5.	PREDICTED SONAR RANGES FOR A SOURCE AT 100 M DEPTH, PROJECTING NORTHWARD.	35

LIST OF FIGURES

Figure 1.	An AVHRR image of the cold filament investigated	8
Figure 2.	The composite sound speed profile calculated at station 133.	9
Figure 3.	A sample output of the PE Acoustic Model for a source propagating southward from station 138	10
Figure 4.	The temperature cross section, from the northern station, 133, to the southern station, 139	20
Figure 5.	The salinity cross section from the northern station, 133, to the southern station, 139.	21
Figure 6.	The density anomaly cross section from the northern station, 133, to the southern station, 139	22
Figure 7.	The geostrophic velocity cross-section from the northern station, 133, to the southern station, 139	23
Figure 8.	The sound speed profile computed at station 133	24
Figure 9.	The sound speed profile computed at station 134	25
Figure 10.	The sound speed profile computed at station 135	26
Figure 11.	The sound speed profile computed at station 136	27
Figure 12.	The sound speed profile computed at station 137	28
Figure 13.	The sound speed profile computed at station 138	29
Figure 14.	The sound speed profile computed at station 139	30
Figure 15.	An overlay plot of the SSPs taken at all the stations. The deep sound channel axis is at 575 m.	31
Figure 16.	A geographical representation of the predicted sonar ranges	36
Figure 17.	A geographical representation of the predicted sonar ranges	37
Figure 18.	A geographical representation of the predicted sonar ranges	38
Figure 19.	A geographical representation of the predicted sonar ranges	39
Figure 20.	The PE Acoustic Model run from station 135 southward to station 139	40
Figure 21.	The PE Acoustic Model run from station 137 to station 133	41
Figure 22.	The PE Acoustic Model run from station 133 to station 139	42
Figure 23.	The PE Acoustic Model run from station 137 to station 133	43
Figure 24.	AVHRR image of a cold filament off NW Africa on 2 July 1985	51
Figure 25.	CZCS image of the region in Figure 24 on 2 July 1985	52

Figure 26. All cold filaments which occurred off South Africa in February 1984 from satellite AVHRR data	53
Figure 27. AVHRR image of a cold filaments off the coast of Portugal on 21 AUG 1979.	54
Figure 28. A schematic diagram of an offshore cold filament. (From The CTZ Group, 1988)	55
Figure 29. Tactical Scenario #1	56
Figure 30. Tactical Scenario #2	57
Figure 31. Tactical Scenario #3	58

I. INTRODUCTION

Oceanic eastern boundary regions have been characterized in the past as broad expanses of slow moving currents (Sverdrup et al., 1942; Picard and Emery, 1982). Recent investigations, aided by satellite imagery, indicate that these regions are far more dynamically active than previously thought, containing frequent mesoscale eddies and cold filaments (Huyer and Kosro, 1987; Flament et al., 1985). These filaments originate in the cold, upwelled, nutrient rich waters along the coast and, crossing the shelf, may extend hundreds of kilometers offshore (Brink, 1983). They present significant gradients of temperature and salinity at their boundaries and may encompass regions of high biological productivity (Lutjeharms, 1987). The filaments are visible from satellites using infrared (IR) imagery from the Advanced Very High Resolution Radiometer (AVHRR), which produces sea surface temperature images; or near-surface ocean color imagery from the Coastal Zone Color Scanner (CZCS) which produces chlorophyll images (Nykaer, 1986). The filaments have been studied in the offshore regions of California, Peru, Portugal, Northwestern Africa, and the west coast of South Africa.

These filaments have been the subject of many recent investigations, but their forcing mechanisms are not yet well understood. Their repeated occurrences at the same locations suggests that they are dynamically tied to topography (Brink, 1983). These cold anomalies may be of particular interest to the U S Navy because, as this study shows, they can contain temperature gradients severe enough to create acoustic fronts. Additionally, they occur frequently in strategically important coastal regions.

These filaments were not extensively studied until satellite imagery became available, however, their presence in the California Current was documented as early as 1939 (Fleming, 1939). More recent studies, now aided by remote sensing, have addressed the

dynamics of these features, and have suggested the following forcing mechanisms. Meso-scale turbulence could provide the driving force for a cold filament by the interaction of a pre-existing eddy field with a coastal boundary (Huyer et al., 1984; Mooers and Robinson, 1984). Dynamic instability is another possibility. Coastal currents may develop filaments by the dynamic instability inherent in the flow (Mysak, 1982; Ikeda et al., 1984; Ikeda and Emery, 1984). The recurrence of these filaments at prominent coastal features provides evidence that high wind stress and irregularities in the coastline and shelf may be responsible (Smith, 1981; Crepon et al., 1984). Bottom topography, particularly sharp sudden features such as the Mendocino Ridge, have also been suggested (Narimousa and Maxworthy, 1987). Structures similar to cold filaments have appeared in dynamical models in response to wind stress (Batteen et al., 1989). Various combinations of the above listed mechanisms are also possible (Atkinson, 1985). Further study is continuing by a variety of researchers.

An extensive study of cold filaments off Pt. Arena was conducted in the California Current System under the auspices of the Coastal Transition Zone (CTZ) program. This program brought together a group of about 34 investigators from twelve institutions to address interdisciplinary descriptive and dynamical questions relating to cold filaments off central California (The CTZ Group, 1989). The preliminary efforts of this group provided a new concept of the structure and kinematics of the flow in the coastal transition zone during the upwelling season. A continuously meandering upwelling jet is now envisioned. A segment of this jet, a "generic" offshore filament, can be identified as a strong baroclinic jet about 40 km wide, flowing offshore at a peak speed of at least 0.5 m s^{-1} , embedded in a field of cyclonic and anticyclonic eddies at a scale of order 100 km (The CTZ Group, 1989). The sampling plan for 1988 was designed to provide more detailed quasi-synoptic spatial and temporal coverage of roughly one meander of the coastal current than had previously been available.

Data acquired during the CTZ88 observation program were used in this investigation. These data were taken from a northwest to southeast transect which crossed a cold filament extending offshore from Pt. Arena, Ca. An acoustic propagation model based on the parabolic equation (PE) was run on this data to determine what effect, if any, the cold thermal anomaly might have on the propagation of sound within its boundaries or in the surrounding waters. The results indicate that the intrusion of the cool waters of the filament into the warmer oceanic waters present a moderate acoustic front. Substantial variation was found between the predicted sonar ranges calculated when a 50, 200, or 800 Hz source was moved from station to station. The longest sonar ranges were found when the acoustic source was located at the station where the coldest sea surface temperatures were observed. This was consistent for all three frequencies and for both source (5 m or 100 m) depths and all three receiver depths (5 m, 100 m and 200 m) investigated. An analysis of the mechanisms resulting in these variations, coupled with descriptions of filaments in other areas (such as Fuiza et al., 1988; Lutjeharms et al., 1987; and Brink, 1983), indicates that filaments of similar dimensions and with similar sea surface temperature gradients could possibly provide similar acoustic frontal features and, hence, be of tactical significance.

II. DATA AND METHODOLOGY

The data for this study were taken as a part of the 1988 CTZ field program. These observations took place between of 6 and 12 July 1988 when historical satellite imagery of this area of the California Current off Point Arena showed the occurrence of a cold filament. Figure 1 shows the satellite sea surface temperature image from 9 July 1988 at 2317 Z, with the CTZ88 station numbers superimposed. Data used in this study were taken at the stations numbered 33 through 39, an offshore transect in deep (~3000 m) water that makes an approximately normal transect across the filament.

A. DATA ACQUISITION

The conductivity, temperature, and depth (CTD) data were taken from the surface to 500 m using a Neil Brown Mark IIIB CTD. The data were acquired using an HP 200 computer and were stored on 3.5 inch diskettes. Raw CTD data were transferred to the IBM 3033 mainframe computer at the Naval Postgraduate School. Temperature and conductivity corrections were applied as described in Jessen et al. (1989) and salinity was calculated from these corrected values according to the algorithm of Lewis and Perkins (1981). Sensor calibration procedures are contained in Jessen et al. (1989). These data were used to determine the fields of temperature, salinity, and density and to construct their vertical profiles. The sound speed was calculated at 5 m increments using the Chen - Millero algorithm (Unesco, 1983).

B. SOUND SPEED PROFILES

Sound speed profiles (SSPs) to 500 m were constructed from the CTZ88 CTD data. Each SSP had to be extended to a depth consistent with the bottom depth in the region, about 3000 m, to allow the deep sound transmission paths to be computed. This was

accomplished by computing an average deep profile produced from 11 deep (3000 m) casts acquired in the area of this study during the OPTOMA 11 cruise (Rienecker et al., 1984). These deep CTD data were also processed at 5 m intervals using the Chen - Millero algorithm, and a sound speed profile from 500 m to 3000 m was produced. This deep SSP was then appended to the bottom of each of the SSPs calculated from the CTZ88 data. The use of this historic deep profile at all of the stations had two beneficial effects for this study:

1. It removed any variation that different bottom depths might have produced by defining the depth as 3000 m at all stations.
2. It also removed any variation that deep temperature structure, not associated with cold filaments, might have produced. At the same time, a representative deep layer was available for input to the model.

In order to use the resulting SSPs with the PE model, it was necessary to reduce the number of points used to describe them. A strobing program was used which compared the computed sound speed at each depth interval with the sound speed of the previous point and selected a profile point only if a predetermined difference was exceeded. This predetermined difference varied with different regions of the SSP. In the top 100 m the difference required to select a new sound speed point was 0.3 m s^{-1} . This ensured that the structure of the mixed layer and upper thermocline was well reproduced. A difference of 1 m s^{-1} was sufficient to describe the lower thermocline down to the level of the sound speed minimum. A difference of 5 m s^{-1} was suitable for the nearly linear region from the depth of the sound speed minimum to the bottom. The sub-sampled SSPs were then compared with the original SSPs to ensure that no significant features had been lost. An example SSP (station 133) is displayed in Figure 2. The SSPs for each station calculated in this manner were entered into the PE acoustic model to provide the environmental background conditions needed by the model.

C. THE PARABOLIC EQUATION ACOUSTIC MODEL

The parabolic equation model is a range-dependent model which determines the propagation of sound through a changing acoustic environment (Kuperman, 1985; Mellberg et al., 1987). It allows varying environmental conditions to be entered at positions along the path of sound propagation. It assumes that the water column, described by a sound speed profile at a given position, remains representative of environmental conditions out to the next position. There, another SSP is entered and

acoustic conditions abruptly change with no smoothing between profiles. The model places the source of acoustic energy at an initial position and source depth. The sound radiates along one line of direction away from this position, traveling through the varying acoustic environments described by the SSPs which are entered along its line of travel. The attenuation of acoustic energy is computed at closely spaced range increments (~ 0.1 km) at distances measured from the source. The distance between stations (SSPs) for the CTZ88 grid was 25 km.

The PE model must consider two complex boundaries, the sea surface and the sea bottom but both boundaries were simplified for this study. Inputs to the model must be provided to describe the bottom in terms of depth and acoustic transmission characteristics. To simplify the effect of the bottom, and to ensure that its effect was consistent from station to station, a constant depth of 3000 m was specified. The bottom was assumed to be fully absorbing (any acoustic energy striking the bottom was completely absorbed) along the entire transmission path. The model assumes a smooth sea surface. This ignores the effects of wind and waves and helps isolate the variation in the predicted sonar ranges to the effects of the cool filament.

The model allows variations of source depth, receiver depth, and source frequency. A total of 252 model runs were performed with the input parameters varied to describe a number of basic hypothetical tactical situations. The model was run with the source depth at 5 m to simulate noise emanating from a surface ship and at 100 m to simulate a submarine-radiated noise source. Frequencies of 50, 200, and 800 Hz were chosen to roughly approximate frequencies of interest in tactical situations. The selection of receiver depths at 5, 100, and 200 m supported the ability of both platforms to listen at various depths.

The model was run with sound projecting down the line of stations from north to south and vice-versa to determine any asymmetry in the propagation of sound across the filament. Model runs from each source depth, each receiver depth and each frequency were done at each station. For a run initiated at any station, the acoustic conditions at each downrange station were evaluated. For the stations at the ends of the line of stations, the conditions prescribed by the SSP for the end station were extended indefinitely.

D. PREDICTED SONAR RANGES

In computing predicted sonar ranges (PSRs) the output of the PE model was organized in a way which allowed direct comparison between model runs and produced

operationally meaningful results. A figure of merit (FOM), the maximum amount of transmission loss which can occur and still allow detection, of 80 dB was chosen and the range to this value was determined graphically from the model output. From each model run up to three PSRs could be determined: the direct path PSR, and the first and second convergence zone PSRs. This results in the possibility of producing five sets of information: the direct path range, the first convergence zone range, the width of the first convergence zone, the second convergence zone range, and the width of the second convergence zone. An example of the output of the PE model (Figure 3) demonstrates the graphical technique used in determining the PSRs.



Figure 1. An AVHRR image of the cold filament investigated: This image was taken on 9 July 1988. The CTZ88 station numbers are superimposed. Stations 33, 34, 35, 36, 37, 38, 39 correspond to stations 133, 134, 135, 136, 137, 138, 139 in this report.

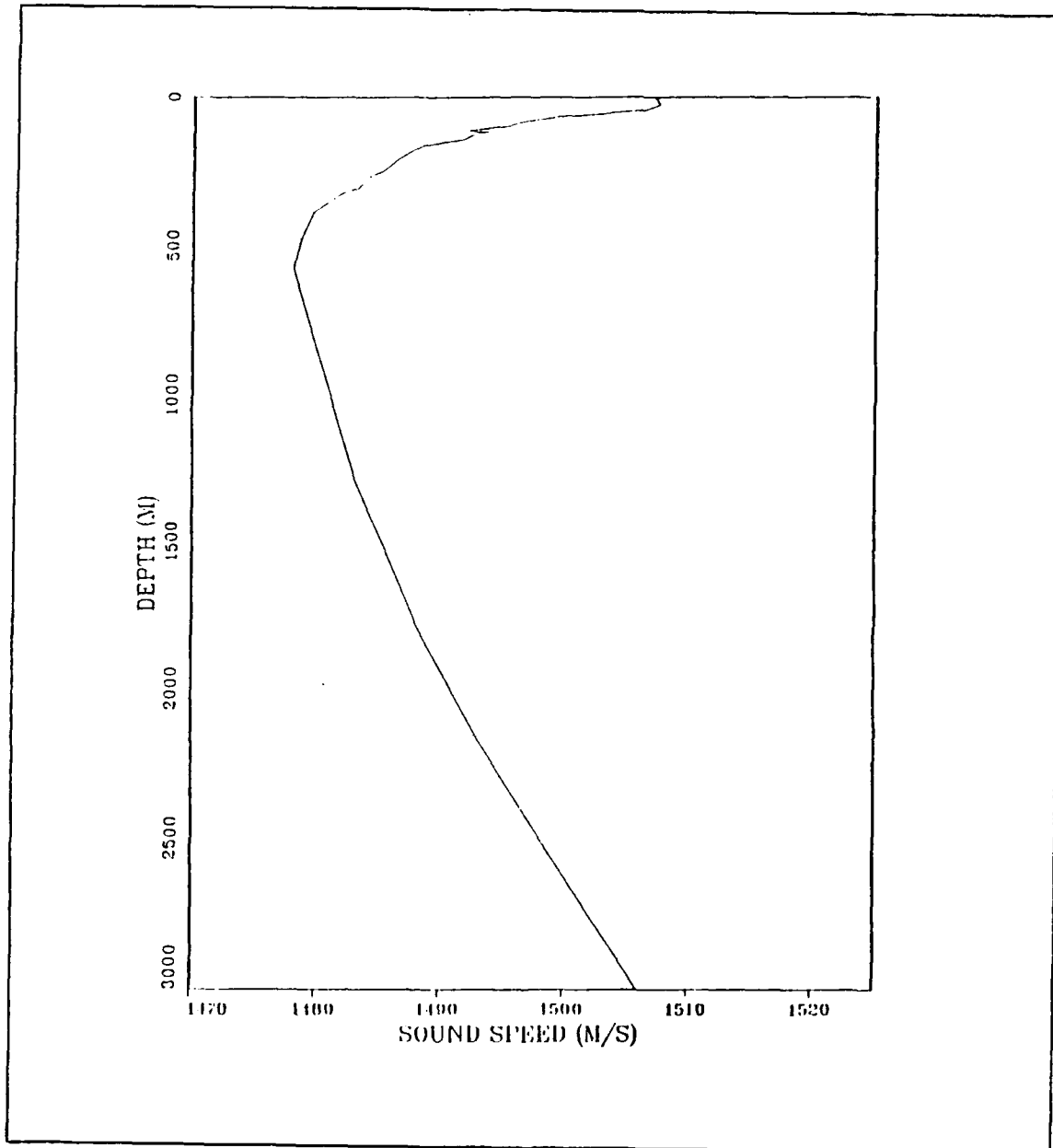


Figure 2. The composite sound speed profile calculated at station 133.

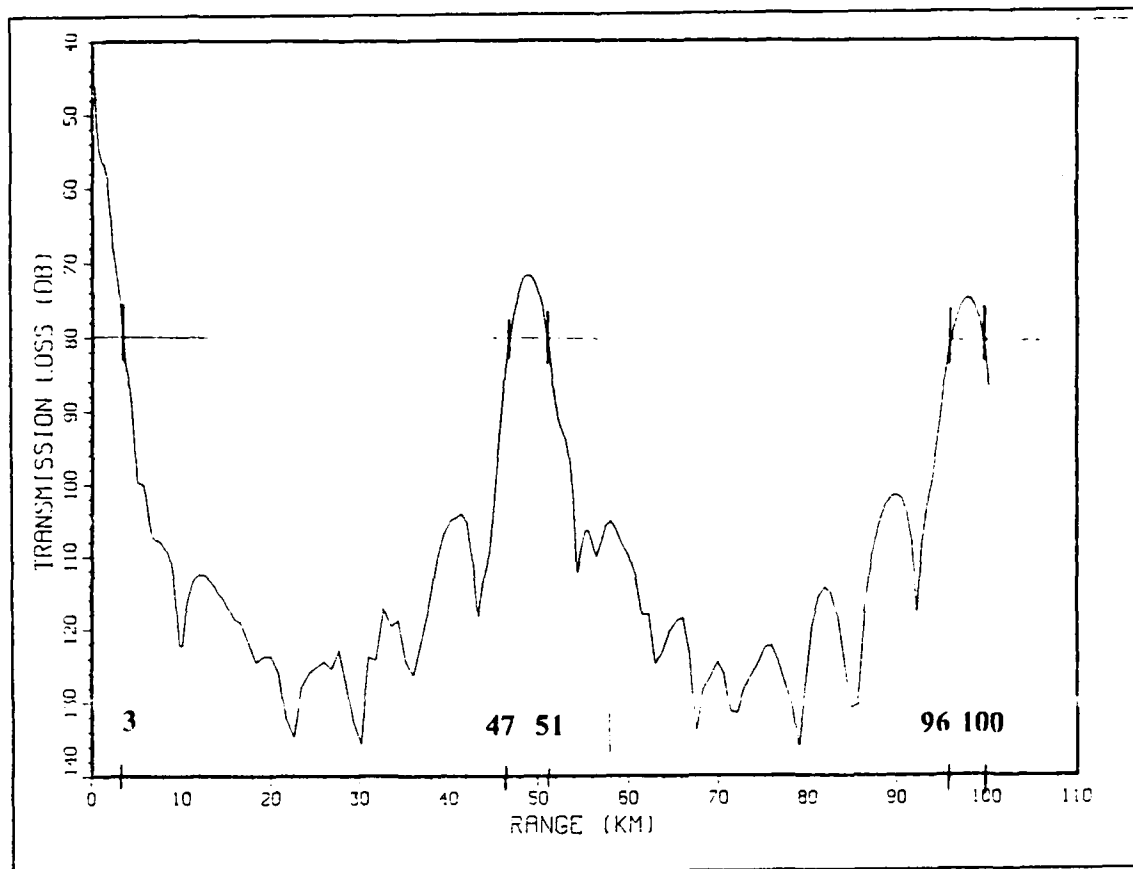


Figure 3. A sample output of the PE Acoustic Model for a source propagating southward from station 138: The source depth was 100 m, the receiver depth was 100 m, and the source frequency was 50 Hz. This demonstrates the direct path range and location of the annuli of the first two convergence zones at 47-51 and 96-100 km.

III. RESULTS

A. A. VERTICAL CROSS SECTIONS

Vertical cross sections of temperature, salinity, density anomaly and geostrophic velocity were constructed (Figures 4, 5, 6 and 7, respectively) for the transect, with station 133, the northernmost station on the left and station 139, the southernmost station on the right (looking onshore).

The temperature cross section (Figure 4) shows that the core of the cold filament was located at station 137 as indicated by the surface temperature minimum of $< 11^{\circ}$ C. The effect of the cold filament on temperature was limited to 75 km horizontally (station 135-138) and to the upper 250 m. The gradient in temperature from station 137 was slightly stronger toward the south ($3^{\circ}\text{C}/25\text{ km}$) than toward the north ($2^{\circ}\text{C}/25\text{ km}$). Also apparent is the elevation in the depth of the mixed layer when progressing from station 133 towards station 137, and its subsidence from station 137 toward station 139. An important feature appeared at station 135 at a depth of 75 m. Interleaving of the cold water from the filament with the warmer oceanic water occurred here at the margin of the filament. This resulted in a layer of warmer water below colder water at about 75 m depth. This situation was conducive to enhanced focusing of sound in the surface duct near this station.

In the California Current System salinity generally increases with depth (Hickey, 1979). Evidence of the filament, since it consisted of upwelled water transported offshore, was expressed as water of increased salinity. A surface salinity maximum of 32.75 (all salinities presented in practical salinity units, PSUs) was observed at station 138 (Figure 5) adjacent to and southward of the temperature minimum observed in Figure 4. The reason for the spatial offset between the temperature minimum and the salinity

maximum is not presently understood. A trend of salinity decreasing to the north was also observed, due to the incursion of lower salinity Pacific Subarctic water from the north into this region (Simpson et al., 1986). The upward slope of the 34.0 isohaline towards the south provides weak evidence that the filament may extend to slightly greater depths than indicated by the temperature section.

A previous study (Flament et al., 1985) found that the temperature and salinity of the southern edge of similar cold offshore filaments in this region were density compensated. The density anomaly cross section (Figure 6) indicated that this was not the situation with this cold filament, which had clearly observable fronts on both its northern and southern boundaries. The geostrophic velocity normal to this section (Figure 7) calculated relative to a level of no motion at 500 dbar showed that the fastest current speeds were offshore at station 136 at $> 0.4 \text{ m s}^{-1}$. The greatest velocity shear was confined to the upper 200 m, but the absolute magnitudes must be interpreted with caution, since 500 dbar may not be a true level of no motion (Daggett, 1989).

B. ANALYSIS OF SOUND SPEED PROFILES

The sound speed profiles were analysed in terms of mixed layer depth, low frequency cutoff and critical depth at each station. The following definitions are provided (Urick, 1983).

Mixed layer depth: The depth of a nearly isothermal surface layer maintained by the action of wind stress on the ocean surface balanced by buoyancy, entrainment from below and viscous dissipation. In this study, the mixed layer depth is defined as the depth where the vertical temperature gradient first exceeded $0.3 \text{ }^{\circ}\text{C}/5 \text{ m}$ depth.

Critical depth: The minimum water depth necessary for surface convergence zone transmission, that is, the depth having the same sound speed as found at the source (or at the near - surface sound speed maximum, whichever is greater).

When these criteria are not met, no critical depth is possible near the surface and that sound speed profile is considered to be bottom limited. For the same sound speed profile the sound speed at 100 m may be slower than the sound speed at 3000 m, and in this case convergence zone ranges could be available for

the deeper source. In this study convergence zone transmission occurred from all stations with the source located at 100 m depth.

Low frequency cutoff: The frequency below which sound is no longer efficiently trapped in the mixed layer. $F_{co} = 2 \times 10^6 \times H^{-1.2}$ where H is the mixed layer depth in meters.

Deep sound channel: A sound transmission channel extending above and below the sound speed minimum.

Figures 8 through 14 illustrate speed profiles derived from the CTD data at stations 133 through 139, respectively. The mixed layer depth (MLD) is included with each profile and also appears with the low frequency cutoff value for each station in Table 1. The existence of a mixed layer depth indicates that surface ducting is possible for source frequencies greater than the cutoff value. For the frequencies used in this study (50, 200 and 800 Hz), the mixed layer depths needed to trap the signals in the surface duct are 238, 96, and 39 m, respectively. Since mixed layer depths > 70 m are rare in the coastal transition zone, it is expected that only the 800 Hz signal will exhibit surface ducting.

Moving through the stations from 133 through 139 (Figures 8 - 14), or from the northernmost to the southernmost station, the SSP at station 133 (Figure 8) showed a mixed layer depth of 43 m. The cutoff frequency of 709 Hz indicated that the source frequencies of 50 and 200 Hz would not be trapped in the mixed layer but the 800 Hz signal would. The critical depth was greater than 3000 m, the model simulated bottom depth at all stations, indicating that convergence zone ranges were not possible for a source at 5 m.

At station 134 (Figure 9) the mixed layer depth was at 71 m. The low frequency cutoff at 335 Hz indicated that the 800 Hz signal could be trapped in the surface layer. The critical depth was too deep to allow convergence zone transmission for a 5 m source.

Station 135 (Figure 10) presented the most interesting SSP. The decrease in sound speed from a depth of 100 m to the surface indicated colder water in that region. This was an expression of the interleaving which occurred at the margin of the cold filament and which provided a layer of colder water over a layer of warmer water. This feature can also be seen in the temperature section (Figure 4) in the 14 ° and 15 °C contours near station 135, at 75 m depth. Comparison with the corresponding salinity section (Figure 5) shows this to be a warm - salty intrusion, with slightly fresher water above. The lack of a corresponding feature in the density anomaly section (Figure 6) indicates a statically stable situation. This temperature inversion acted to reinforce the focusing

of sound transmitted in the mixed layer. Surface ducted sonar ranges were expected at this station because of this feature. The low frequency cutoff at 335 Hz indicated that only the 800 Hz signal could be completely trapped in the mixed layer. CZ transmission was not expected for a 5 m source because the critical depth was greater than 3000 m.

At station 136 (Figure 11) the surface temperature decreased under the influence of the cold filament. A substantial reduction in the depth of the mixed layer to 31 m was also observed. With a low frequency cutoff of 1164 Hz, reduced direct path ranges were expected for all of the frequencies of interest. The critical depth rose to 2500 m making CZ transmission possible for both a 5 m and a 100 m source.

The SSP at Station 137 (Figure 12) demonstrated the effects of the coldest water of the filament. The mixed layer depth of 41 m resulted in a low frequency cutoff of 761 Hz which could marginally influence the 800 Hz signal but could not trap the 50 and 200 Hz signals. The lowest surface temperature at this location resulted in the lowest near surface sound speed and the shallowest critical depth of all stations at 1850 m. This was expected to ensure convergence zone transmission at all source depths.

At station 138 (Figure 13) the surface waters were warmer than in the cold filament core to the north. The surface duct was very shallow at 26 m limiting the mixed layer transmission to frequencies above 1508 Hz. The critical depth was shallow enough at 2600 m to allow CZ transmission for a source located at either 5 m or 100 m depth.

At station 139 (Figure 14) the surface temperature and surface sound speed increased. The mixed layer was deeper than station 138, extending to a 41 m depth. The low frequency cutoff of 761 Hz allowed some trapping of the 800 Hz signal. A critical depth of 2650 m allowed CZ transmission for a source located at 5 m or 100 m depth.

All of the sound speed profiles were overlaid (Figure 15) to demonstrate the spatial variability of the SSPs. The SSPs fell into three groups, identified as A, B, and C. Group A consisted only of the SSP at station 137 which stood alone with the lowest surface sound speed. This occurred near the core of the cold water filament. Here the surface sound speed was approximately 18 m/sec slower than the highest surface sound speeds indicated on the the Group C SSPs. At station 137 convergence zone transmission was expected at all source depths.

The stations in Group B included stations 136, 138, and 139. Stations 136 and 138 are in the filament margins where isotherms slope sharply upwards toward the surface resulting in a shallow mixed layer depth. The mixed layer depth at station 139 to the south was also shallower than those found to to the north. The shallow mixed layer depth and relatively warm temperatures cause this group of stations to have SSP prop-

erties intermediate between those of Group A and Group C, that is, weak surface duct direct path transmission but with CZ transmission for a 5 m source.

The SSPs to the north of the filament, identified as Group C, were stations 133, 134, and 135. These SSPs were similar in their relatively deep mixed layer and relatively high near-surface sound speeds. The deep mixed layers served to extend direct path ranges at 800 Hz while the high surface temperatures acted to drive down the critical depth and preclude CZ transmission for a 5 m source.

To summarize, the sound speed profiles for stations 133 - 139 (Figures 8-14) clearly were affected by the presence of the cold filament. Between stations 136 and 137 the critical depth rose from 2500 m to 1850 m for a change in critical depth of 650 m in 25 km, indicating that the cold filament in this study did present an acoustic front, defined as a change in critical depth of 50 m or more over a distance of 35 km (Cheney, 1976). The influence of this front on acoustic propagation is investigated subsequently using the PE model.

C. RESULTING PREDICTED SONAR RANGES

The PSRs calculated from all the model runs done to support this investigation are shown in Tables 2 - 5. Tables 2 and 3 contain PSRs from the runs projecting southward from each station. Table 2 was produced with the source at 5 m, and Table 3 with the source at 100 m. Tables 4 and 5 were constructed from the runs projecting northward from each station. Table 4 was produced with the source at 5 m and Table 5 with the source at 100 m. When two PSRs are present, e.g., 49/51, this indicates the inner and outer edges of the CZ annulus. Zone widths of less than 1 km have identical CZ ranges e.g., 100/100.

In order to make the PSR data easier to interpret, the table data which best characterized the effects of the acoustic front were graphically displayed (Figures 16-19) as plan-views which show the PSRs in the context of the geographical separation of the stations. The stations are labeled across the top and bottom of each figure. The solid circle below the station number indicates the source originates at that station. Extending from each dot are arrows pointing in both horizontal directions. These arrows represent the direct path ranges available at each station with the actual distance in kilometers indicated above each dot. The distance to the inner and outer edges of the convergence zones are indicated by vertical bars (with actual distances shown above) connected with horizontal dashed lines, i.e., the source can be heard (to the 80 dB FOM)

within the bars. These figures are useful in examining the differences in PSRs which occurred from station to station.

1. Variation of PSRs with frequency

1. The longest direct path ranges from a shallow source (Tables 2 and 4) occurred at the highest frequency, 800 Hz. This was because the surface mixed layer was sometimes very effective at trapping the 800 Hz signal, but not the 50 or 200 Hz signals (Table 1).
2. When the source and receiver were at the same depth, convergence zones occurred most frequently at the lowest (50 Hz) frequency (Figures 16 and 17). The direct path, first CZ and second CZ ranges were available at all stations in both directions (Figure 16). This is an expression of lower spreading losses at 50 Hz.
3. The most convergence zone transmissions, when the receiver was at 200 m and the source was at 100 m. (Tables 3 and 5) occurred at 200 Hz. This was because the 50 Hz signals suffered greater duct loss and the 800 Hz signals greater absorption loss.

2. Variation of PSRs with receiver depth

Tables 2 and 4 show that the longest ranges for shallow sources of all frequencies occurred at the deepest receiver depth. This is probably due to image interference at the surface. Sound arriving at the deepest receivers was less susceptible to phase cancellation while sound arriving at the shallow receivers was more subject to surface decoupling losses, i.e., increased phase cancellation with decreasing receiver depth.

3. Variation of PSRs with mixed layer depth

Longer direct path ranges occurred for shallow sources located at stations in the filament and to the north (Figures 17 and 19). This was due to the warm, salty intrusion at station 135 (see below) combined with a deeper mixed layer depth to the north which trapped more energy in the surface duct.

4. Variation of PSRs with surface temperature

Second convergence zone ranges were available for sources near the surface in the cold waters of the filament but not in the surrounding warmer waters (Figure 17 and 19). This is the result of raising the critical depth by a decrease in surface temperature to the point where fewer bottom losses occurred. Energy was focused into the convergence zone path and extended the range to the second CZ.

5. Variation in PSRs due to shallow SSP structure

The longest direct path surface duct ranges occurred at station 135 (Figure 17). The shape of the transmission loss curve from the source to 26 km (Figure 20) indicated that the surface ducting occurred due to the unique shape of the SSP at station 135. The 26 km range may possibly be erroneous, caused by the PE model which extends the

environmental conditions at one station to the location of the next station and then changes them abruptly. The true extent of this surface duct would be the true extent of the SSP at station 135. This was not resolved by the 25 km station spacing.

6. Variations in PSRs showing acoustic asymmetry across the front

The CZ transmission toward the north from station 137 resulted in a convergence zone annulus 16 km wide (Figure 17). This was significantly wider than the width of the corresponding band at the station to the south, station 138, which had a convergence zone 3 km wide. The transmission loss curve for station 137 toward the north (Figure 21) showed evidence of surface ducting. The shape of the curve and its similarity to the direct path conditions at station 135 (Figure 20) suggested that the sound transmitted from station 137 reached the surface at station 135 via a convergence zone path where it was then trapped in the mixed layer and traveled via the surface duct.

The mechanism of expansion of the depth span of the convergence zone ray path was indicated in another asymmetric situation. When projecting southward across the front from station 133, no convergence zone reception occurred for a shallow receiver at a distance of 50 km (near station 135) but a CZ did occur at 99 km. At station 133, with the source at 100 m, and at a source frequency of 800 Hz projecting northward towards receivers at 5 m depth (Figure 18), only direct path transmission was available. This was because the sound speed at the source (station 133, 100 m depth) at 1492 m s^{-1} is significantly less than the sound speed at the receiver (station 133 SSP conditions displaced 50 km to the north, at 5 m depth), at 1507 m s^{-1} and the convergence zone rays are directed toward the bottom before they reach the receiver at 5 m. When projecting from station 133 with an 800 Hz source at 100 m depth toward the south an equivalent situation was encountered at station 135. The sound speed at the location of a receiver 5 m deep is significantly higher at 1503 m s^{-1} than the sound speed at the source and there is no convergence zone transmission. Continuing southward to station 137 presents a substantial variation in SSP. At station 137 the sound speed at a 5 m receiver (1489 m s^{-1}) is less than the sound speed at the source (1492 m s^{-1}), the depth band of the convergence zone ray path is expanded to include the 5 m receiver and convergence zone transmissions were received at the shallow receiver.

In a reciprocal situation, that is, projecting northward from a source placed at station 137 (Figure 19), a CZ range existed at 50 km near station 135. This appears to occur because the conditions for focusing the CZ transmission at station 137 were so much more favorable, as indicated by the shallow critical depth there, that the strength

of the CZ signal overpowers the effect of the poor convergence environment at station 135 (Figure 23).

In summary, the effect of the cold filament on PSRs is to cause substantial variation in sonar range capabilities, particularly at shallow depths, depending on the positions of both the source and the receiver relative to the cold water filament. These variations, while explained by several different mechanisms, are all due to variations in the SSPs in the upper 100 m brought about by the incursion of the cold water filament into the warmer oceanic waters.

Table 1. MIXED LAYER DEPTH AND LOW FREQUENCY CUTOFF AT EACH STATION.

STATION ID	133	134	135	136	137	138	139
MLD (m)	43	71	71	31	41	26	41
F_m (Hz)	709	335	335	1164	761	1508	761

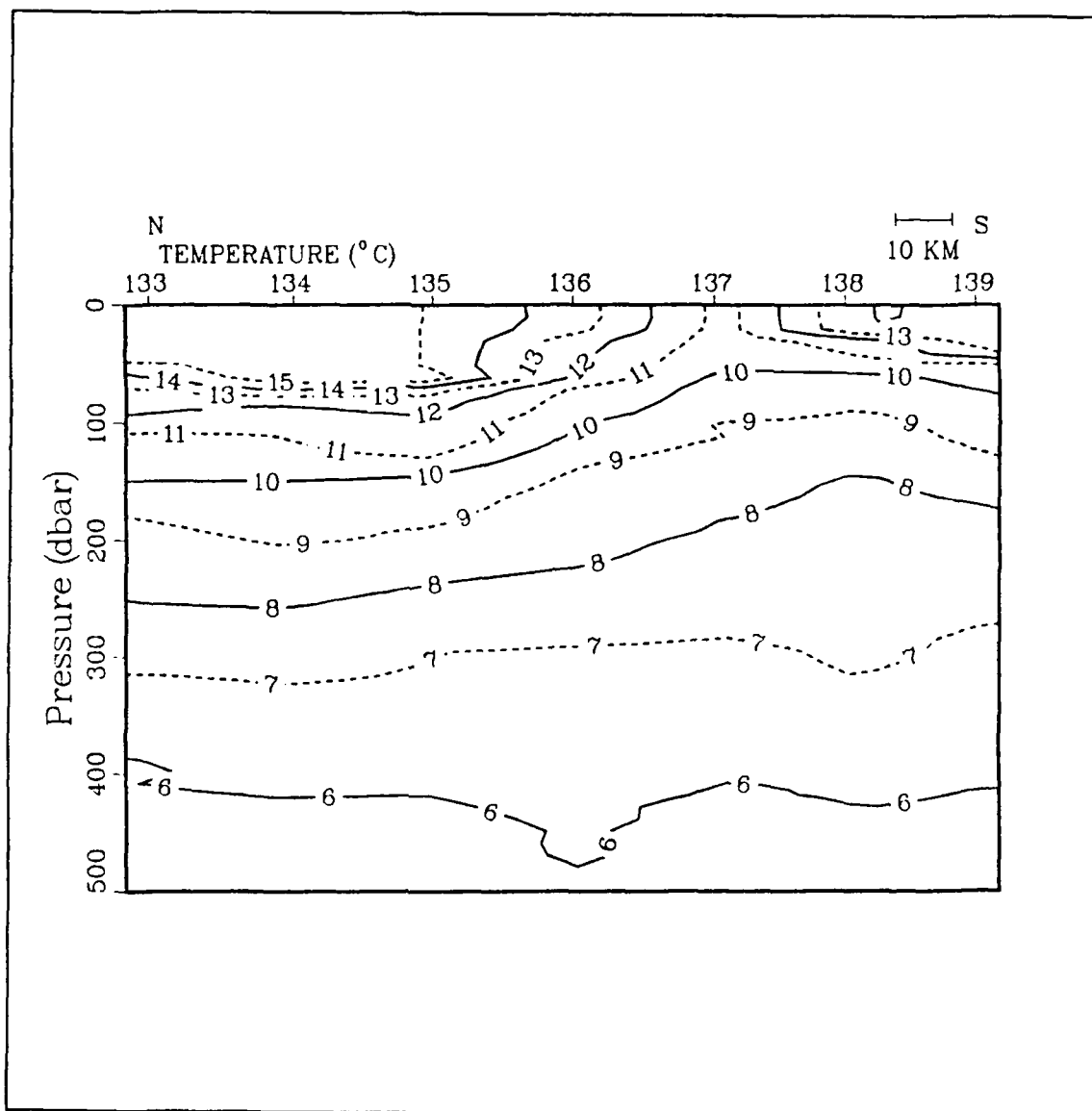


Figure 4. The temperature cross section, from the northern station, 133, to the southern station, 139.

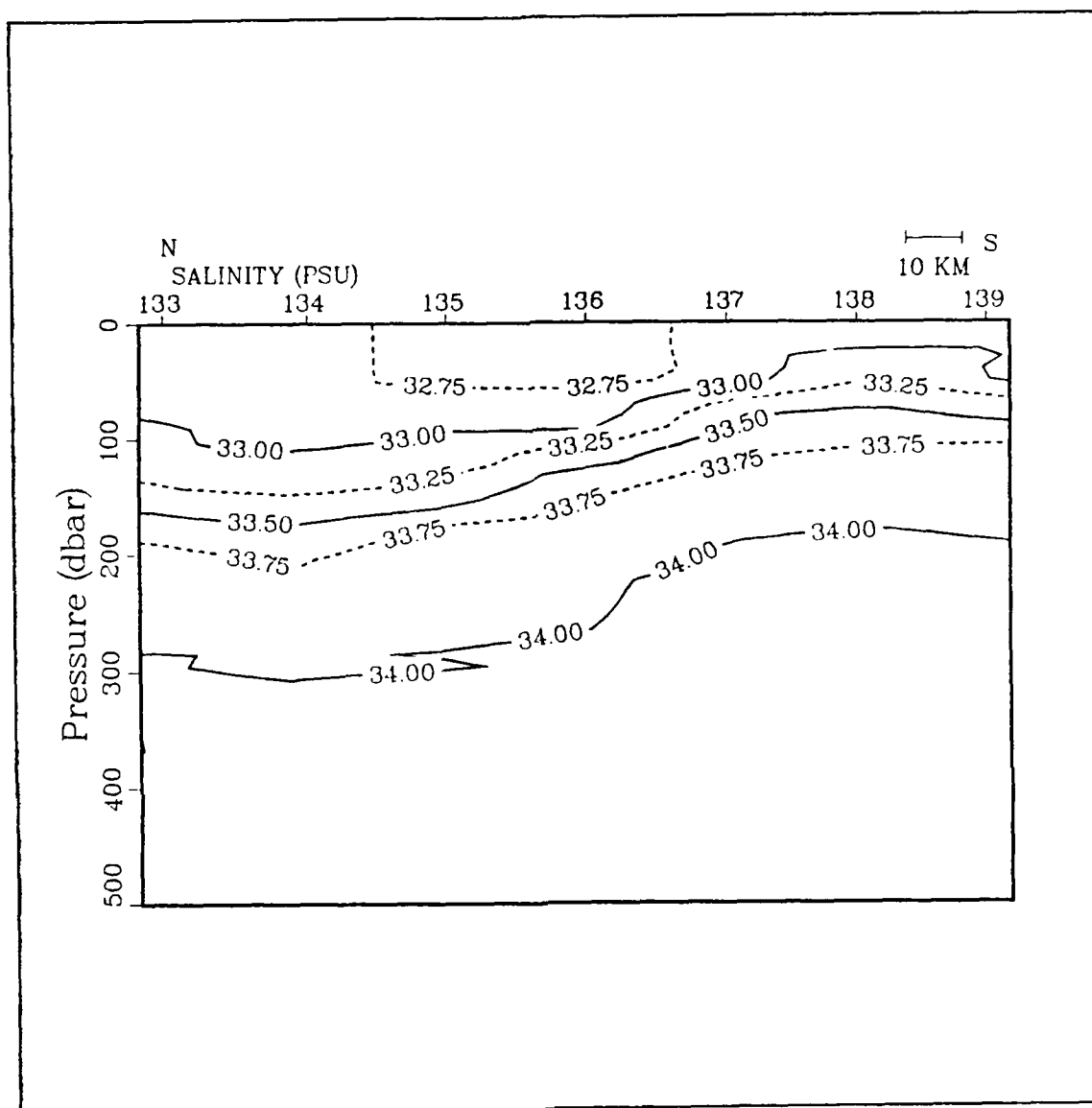


Figure 5. The salinity cross section from the northern station, 133, to the southern station, 139.

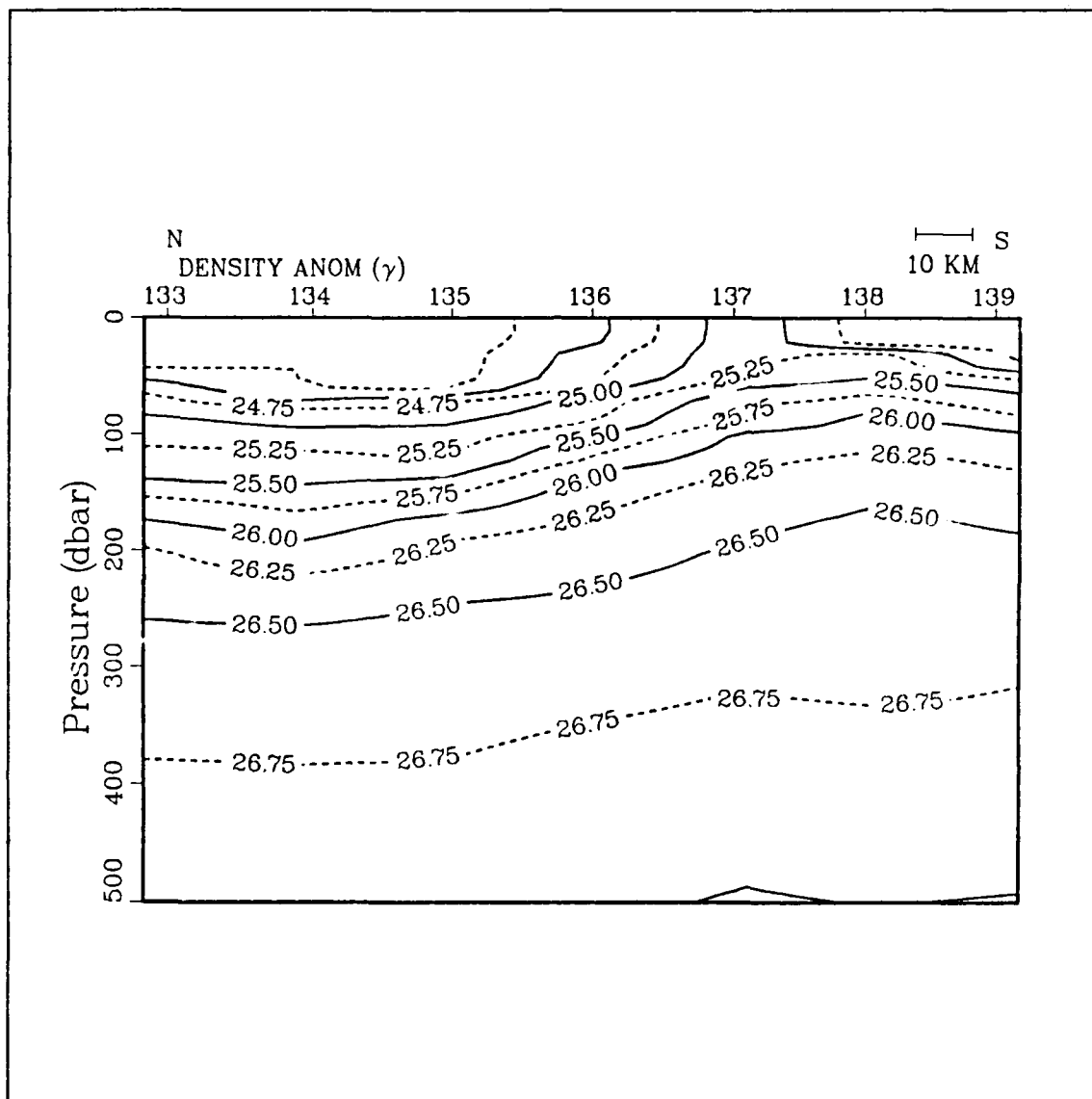


Figure 6. The density anomaly cross section from the northern station, 133, to the southern station, 139.

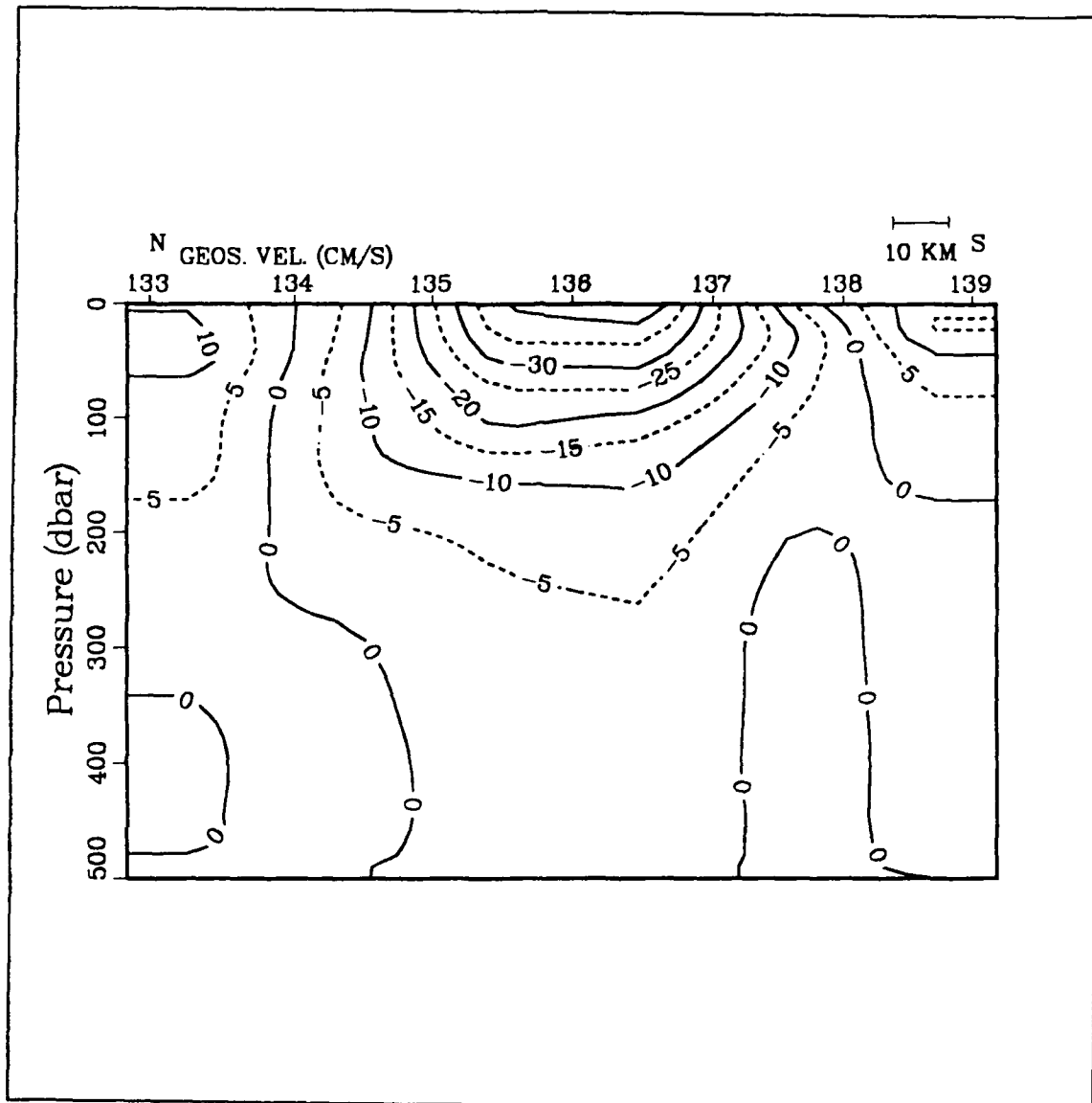


Figure 7. The geostrophic velocity cross-section from the northern station, 133, to the southern station, 139: Negative velocities are out of the page (westward) and positive velocities are into the page (eastward).

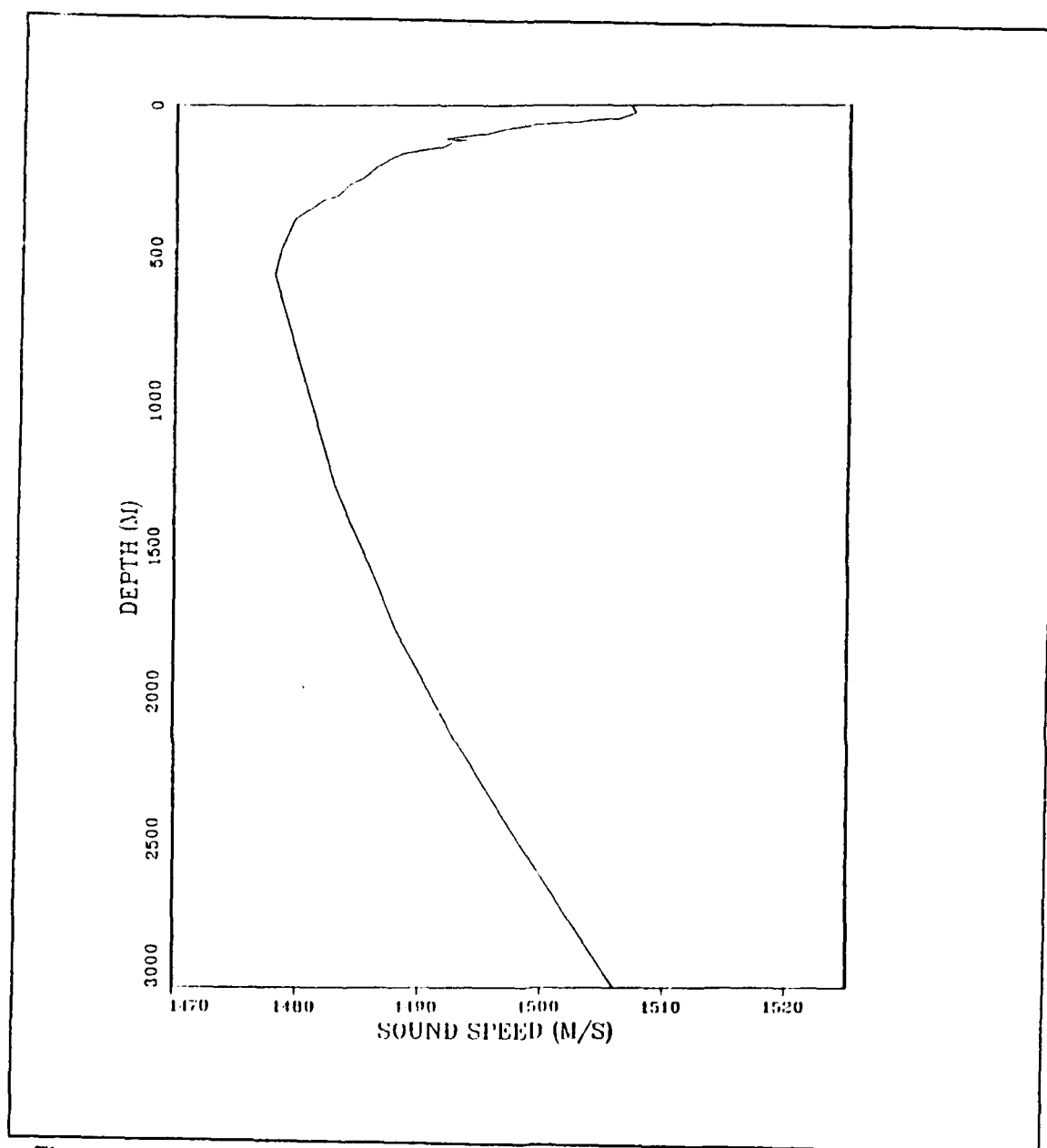


Figure 8. The sound speed profile computed at station 133: The mixed layer depth is 43 m.

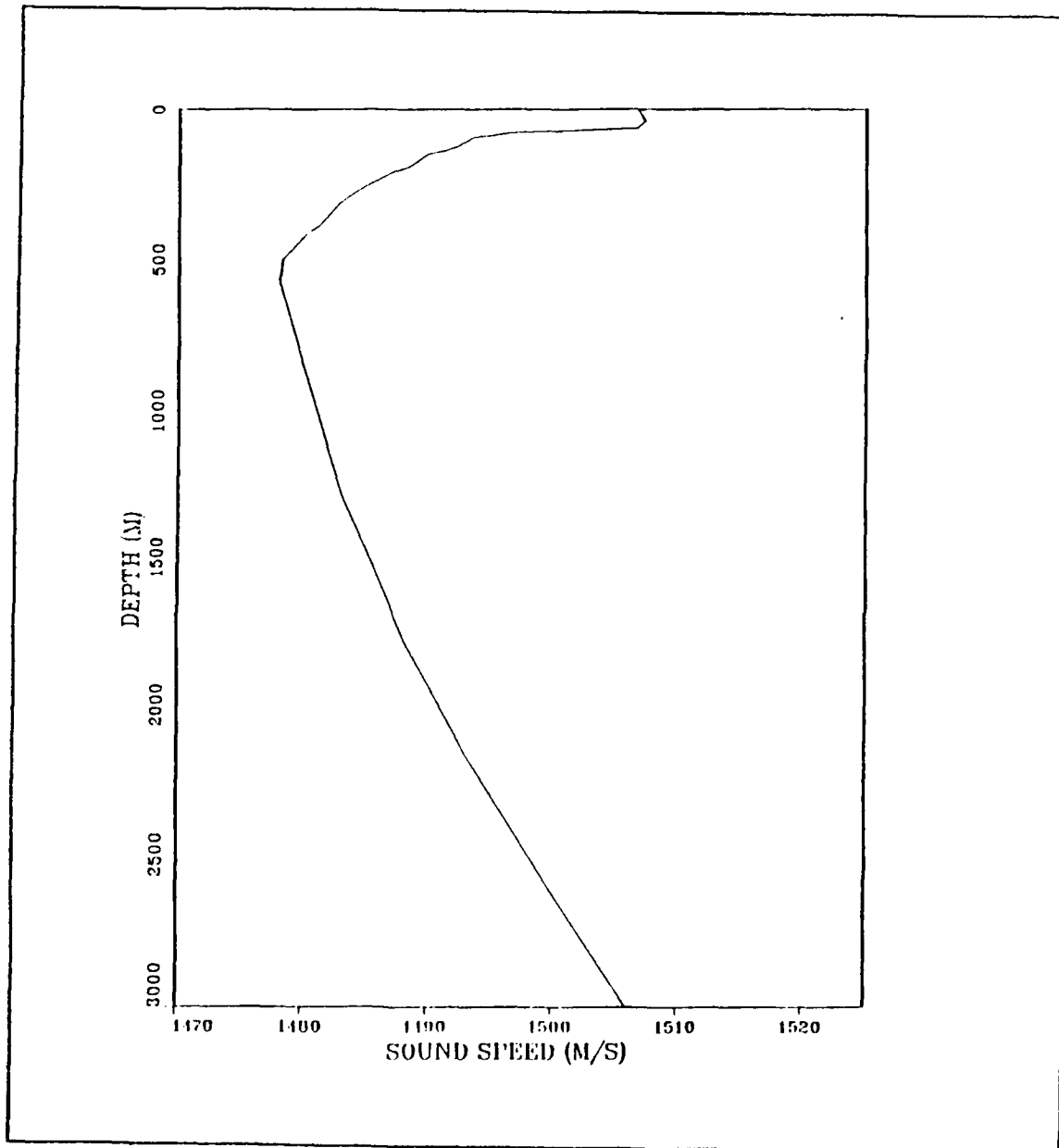


Figure 9. The sound speed profile computed at station 134: The mixed layer depth is 71 m.

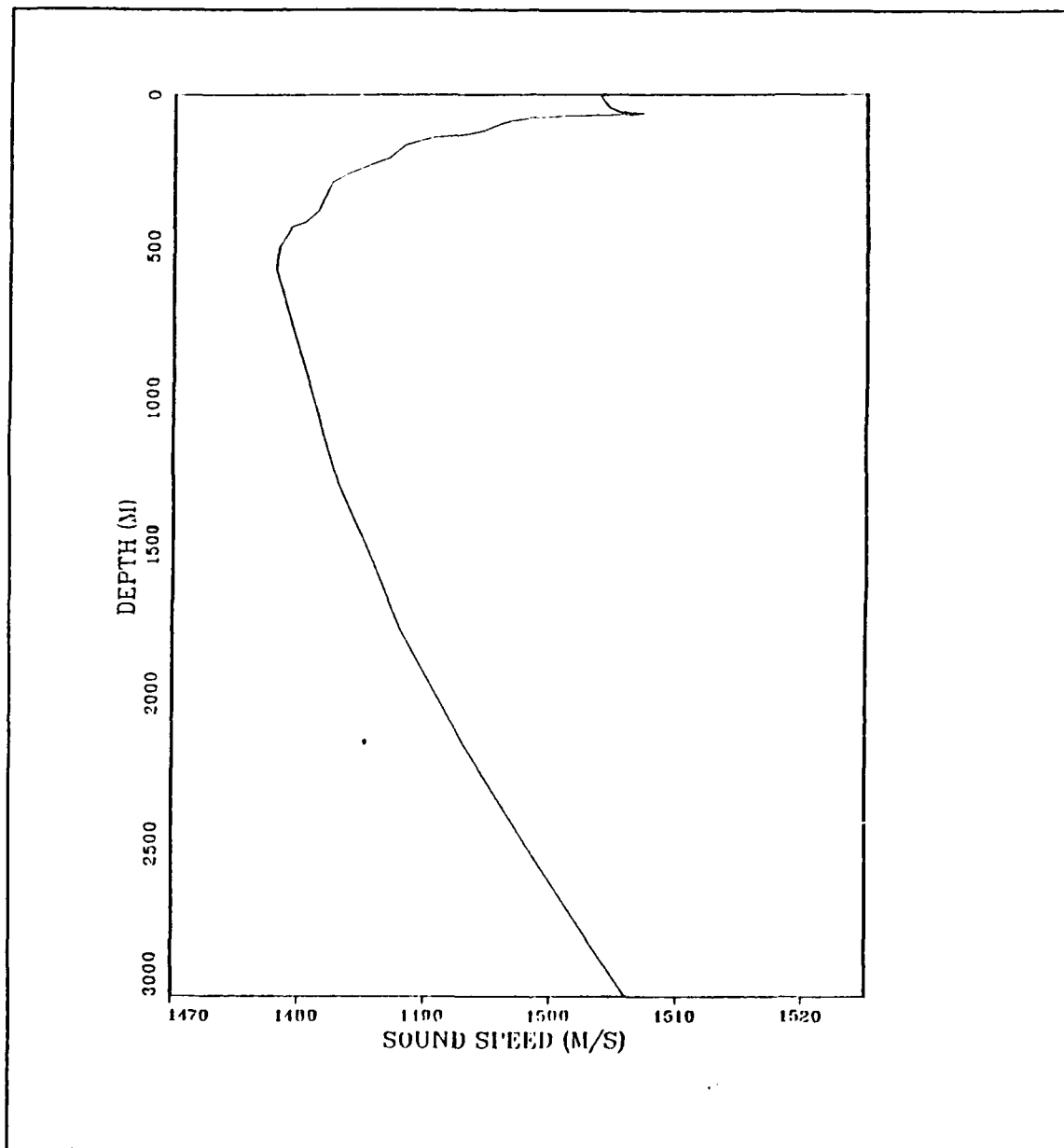


Figure 10. The sound speed profile computed at station 135: The mixed layer depth is 71 m.

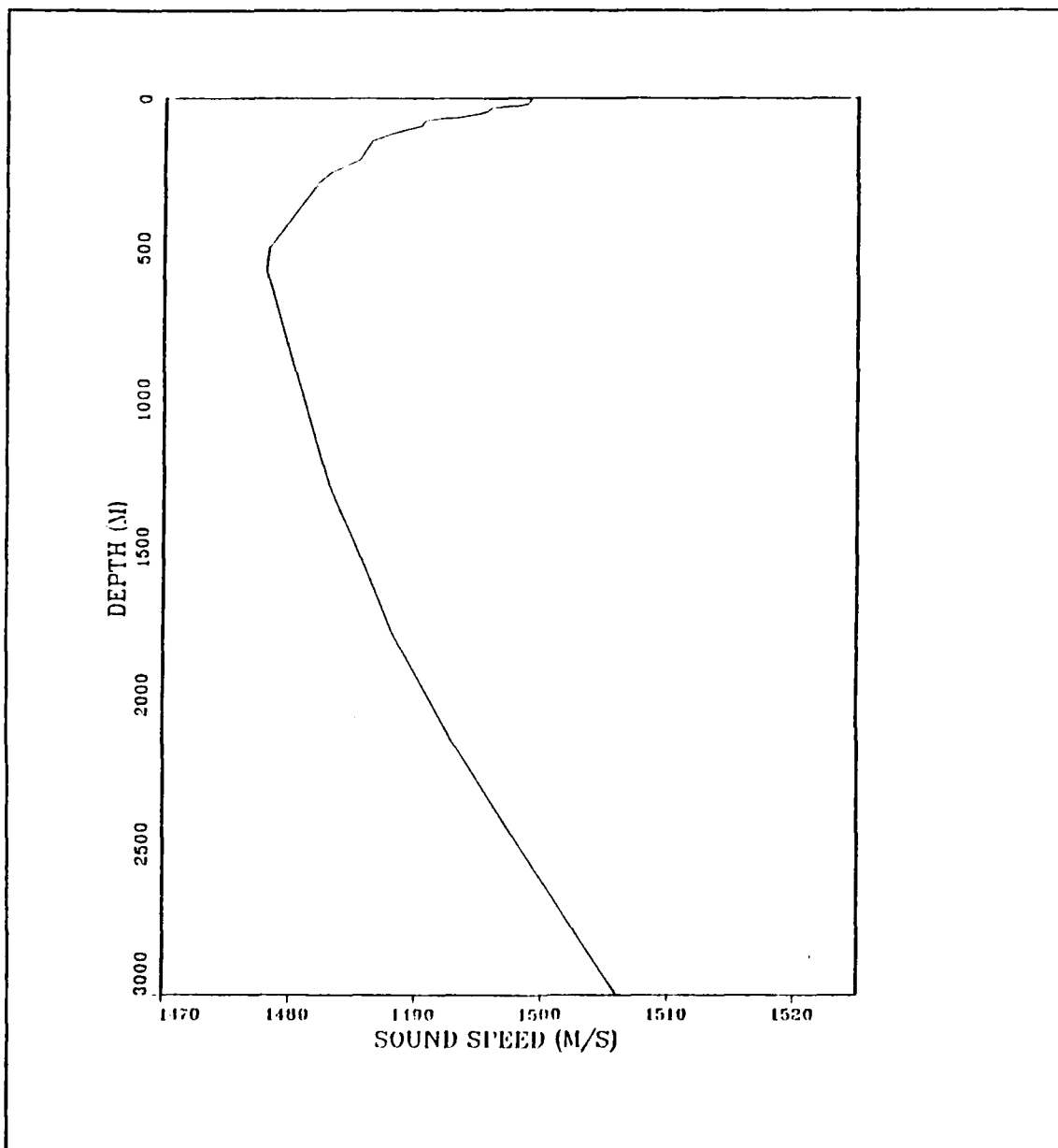


Figure 11. The sound speed profile computed at station 136: The mixed layer depth is 31 m.

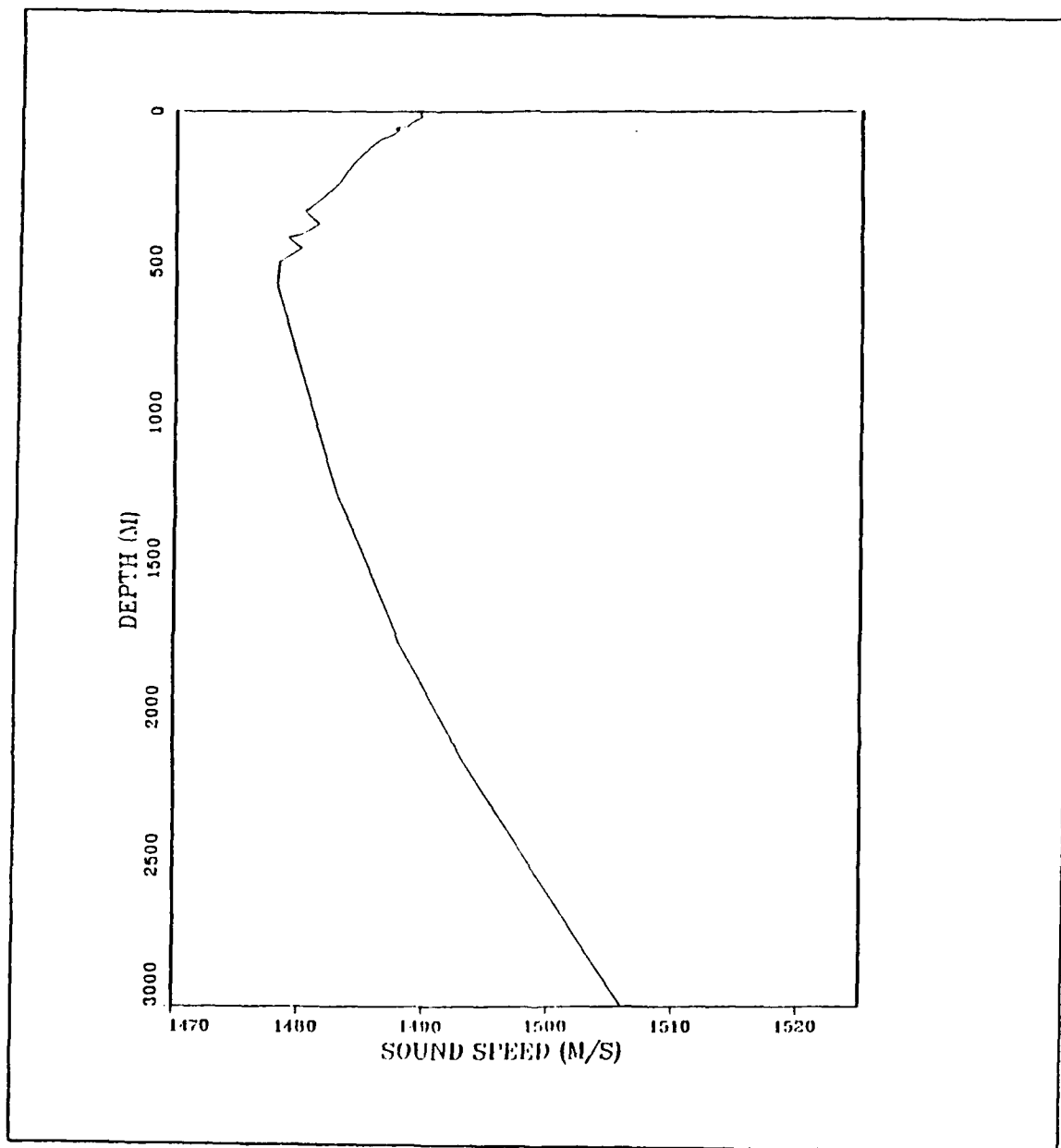


Figure 12. The sound speed profile computed at station 137: The mixed layer depth is 41 m.

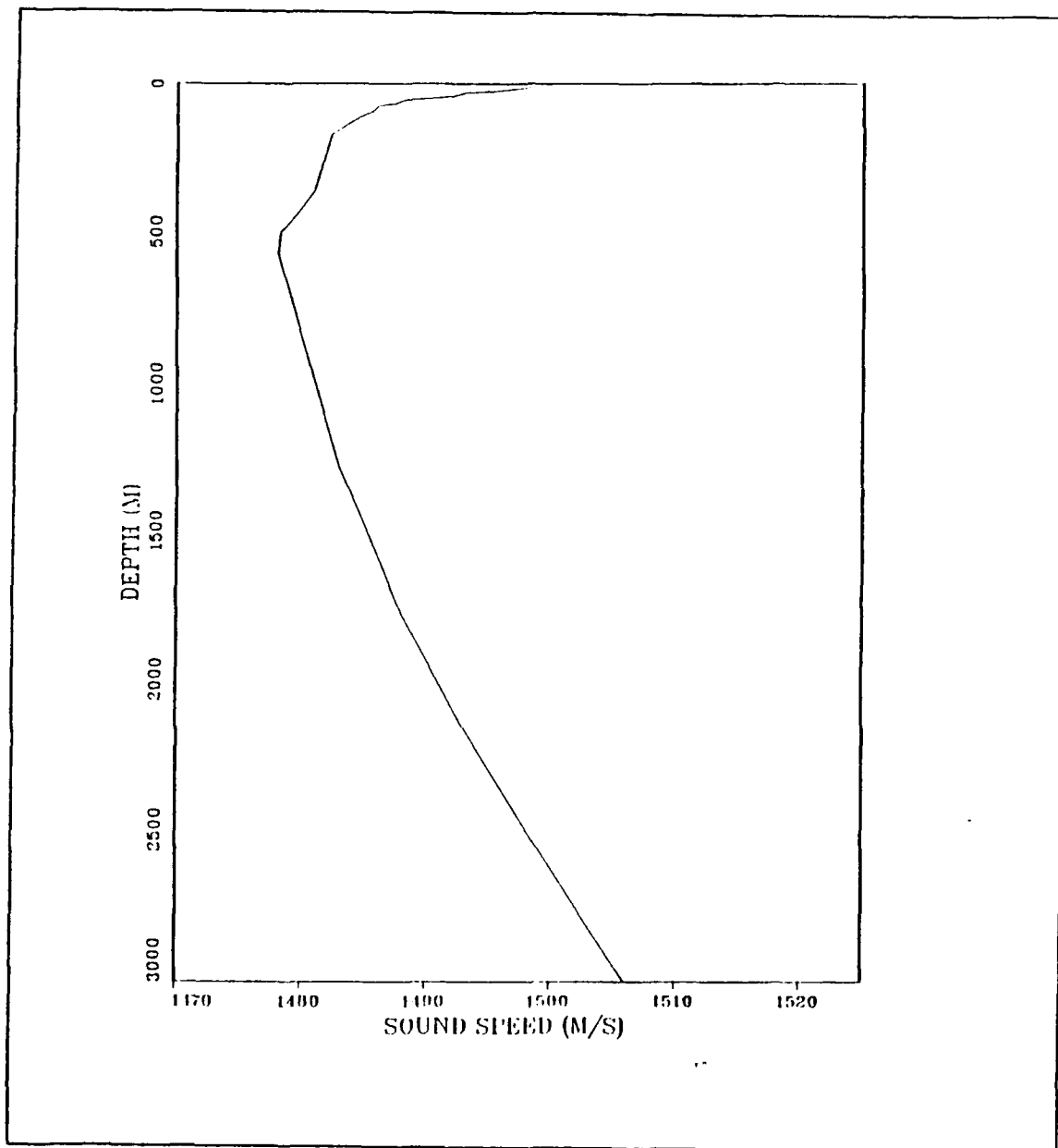


Figure 13. The sound speed profile computed at station 138: The mixed layer depth is 26 m.

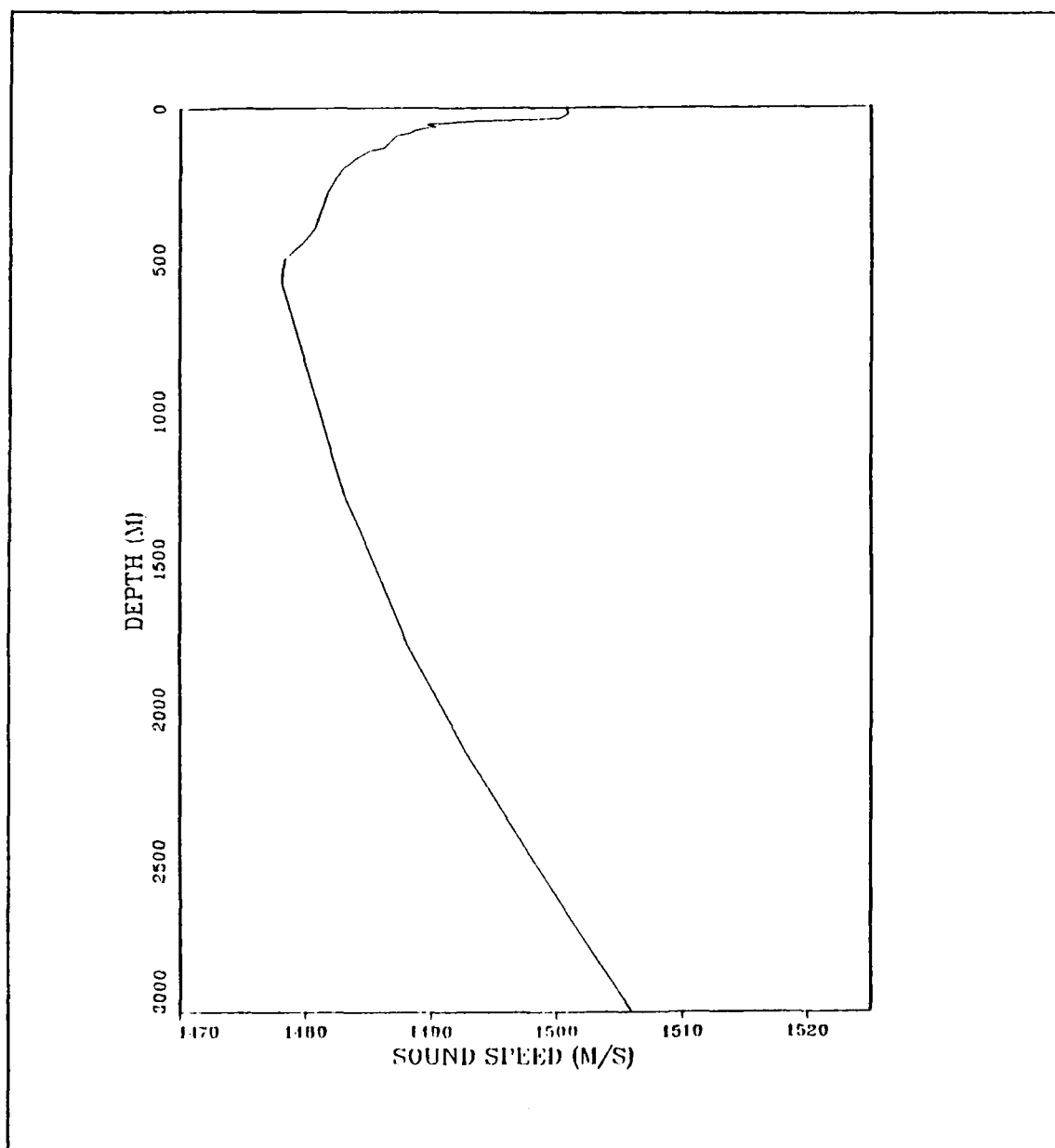


Figure 14. The sound speed profile computed at station 139: The mixed layer depth is 41 m.

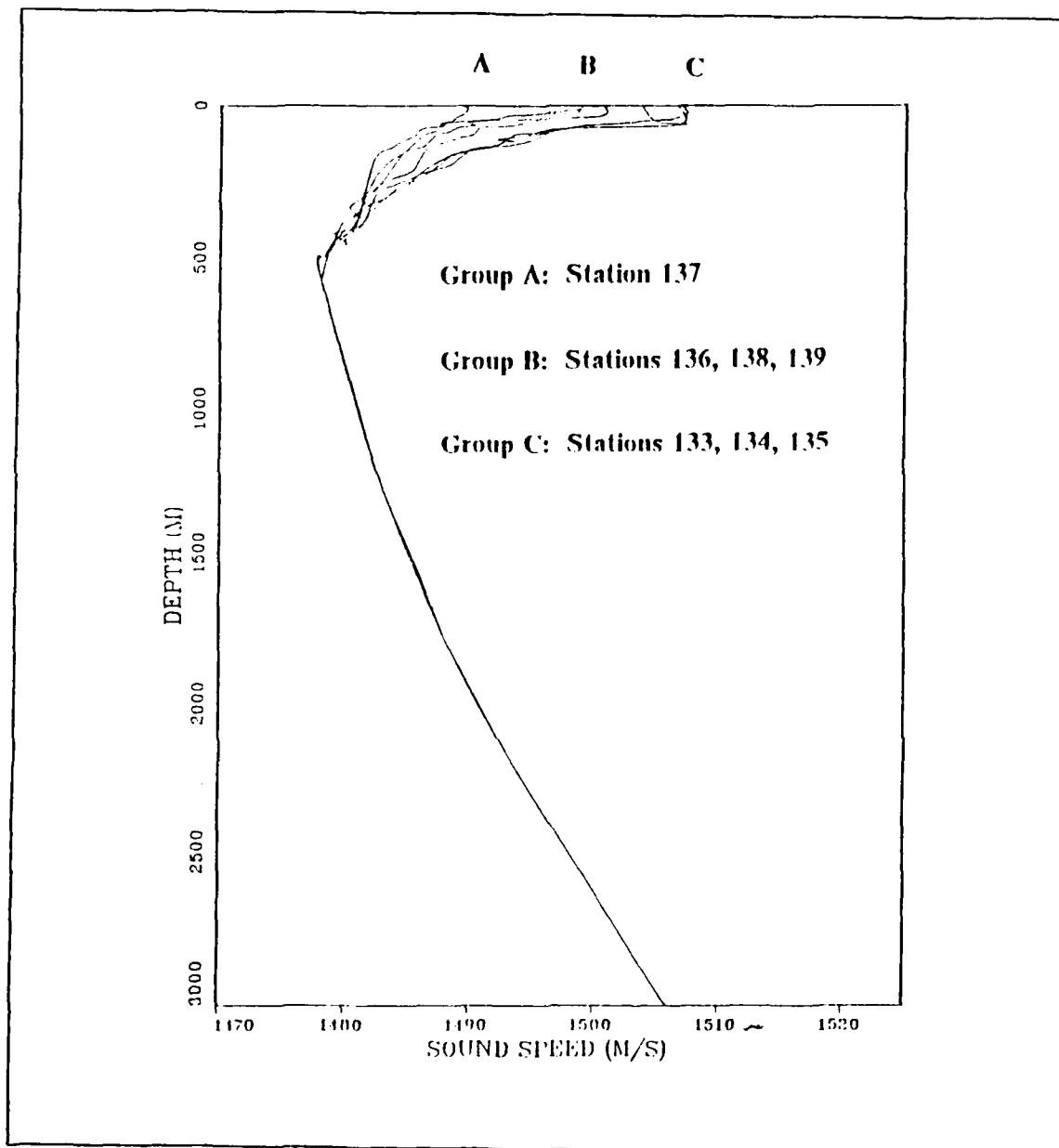


Figure 15. An overlay plot of the SSPs taken at all the stations. The deep sound channel axis is at 575 m.

Table 2. Predicted sonar ranges for a source at 5 m depth and projecting southward when the source is located at each of the stations indicated. A (-) indicates no CZ.

Station ID	133			134			135			136			137			138			139		
Frequency (Hz)	50	200	800	50	200	800	50	200	800	50	200	800	50	200	800	50	200	800	50	200	800
Receiver Depth, Sound Path	Predicted Sonar Ranges (km)																				
5m, Direct	1	1	2	1	1	4	1	1	1	26	1	1	2	1	1	3	1	1	1	1	2
5m, 1st CZ	-	-	-	-	-	-	-	-	-	-	-	-	49/51	-	-	49/50	-	-	50/51	-	-
5m, 2nd CZ	-	-	-	-	-	-	-	-	-	-	-	-	-	-	-	100/100	-	-	-	-	-
100m, Direct	2	2	4	2	2	4	2	2	2	5	2	2	3	2	2	3	2	2	2	2	3
100m, 1st CZ	-	-	-	-	-	-	-	-	-	26/26	-	-	49/51	-	-	48/51	48/51	-	49/52	-	-
100m, 2nd CZ	-	-	-	-	-	-	-	-	-	-	-	-	-	-	-	-	-	-	-	-	-
200m, Direct	3	2	4	2	2	4	2	2	2	5	2	2	4	2	2	4	2	2	2	2	4
200m, 1st CZ	-	-	-	-	-	-	-	-	-	27/27	-	-	48/52	-	-	47/51	47/52	-	49/51	-	-
200m, 2nd CZ	-	-	-	-	-	-	-	-	-	-	-	-	-	-	-	96/100	-	-	-	-	-

Table 3. Predicted sonar ranges for a source at 100 m depth and projecting southward when the source is located at each of the stations indicated. A (-) indicates no CZ.

Station ID	133			134			135			136			137			138			139		
Frequency (Hz)	50	200	800	50	200	800	50	200	800	50	200	800	50	200	800	50	200	800	50	200	800
Receiver Depth, Sound Path	Predicted Sonar Ranges (km)																				
5m, Direct	2	3	4	2	2	4	2	2	5	2	2	3	2	2	3	2	2	2	2	2	3
5m, 1st CZ	-	-	99/100	-	-	97/99	-	-	49/51	-	48/49	48/52	-	-	49/51	-	-	49/54	-	-	49/52
5m, 2nd CZ	-	-	-	-	-	-	-	-	-	-	-	-	-	-	-	-	-	-	-	-	-
100m, Direct	3.0	4	4	3	4	4	3	4	4	5	3	4	4	4	4	6	3	3	3	4	4
100m, 1st CZ	50/52	48/50	48/52	48/52	48/48	48/52	48/51	50/51	48/53	47/51	47/52	47/52	47/52	47/54	47/54	47/51	47/53	49/49	47/52	47/52	47/52
100m, 2nd CZ	97/100	97/100	98/98	98/100	96/99	96/99	98/99	97/100	98/100	97/100	98/101	97/100	96/100	96/99	98/100	96/100	96/100	-	96/100	95/100	96/99
200m, Direct	4	4	4	4	4	5	4	5	4	4	4	4.8	6	6	7	4	4	5	4	4	6
200m, 1st CZ	47/52	47/52	47/52	47/52	47/52	46/52	47/52	47/52	47/53	47/52	46/53	48/53	46/53	48/54	46/53	46/53	46/53	46/52	46/53	46/54	46/54
200m, 2nd CZ	100/100	96/100	-	-	95/100	93/96	-	96/97	-	96/100	96/97	97/98	96/100	98/100	98/98	95/98	96/100	95/97	95/101	95/99	99/99

Table 4. Predicted sonar ranges for a source at 5 m depth and projecting northward when the source is located at each of the stations indicated. A (-) indicates no CZ.

Station ID	139			138			137			136			135			134			133		
	50	200	800	50	200	800	50	200	800	50	200	800	50	200	800	50	200	800	50	200	800
Receiver Depth, Sound Path	Predicted Sonar Ranges (km)																				
5m. Direct	1	1	2	1	1	1	1	1	3	1	1	1	1	1	26	1	1	4	1	1	2
5m. 1st CZ	-	-	50/51	-	-	49/51	-	-	50/65	-	-	-	-	-	-	-	-	-	-	-	-
5m. 2nd CZ	-	-	-	-	-	-	-	-	-	-	-	-	-	-	-	-	-	-	-	-	-
100m. Direct	2	2	3	2	2	2	2	2	3	2	2	2	2	2	5	2	2	4	2	2	4
100m. 1st CZ	-	-	50/51	-	-	50/52	-	48/51	48/52	-	-	49/51	-	-	-	-	-	-	-	-	-
100m. 2nd CZ	-	-	-	-	-	-	-	-	98/99	-	-	98/99	-	-	-	-	-	-	-	-	-
200m. Direct	2	2	4	2	2	2	2	4	5	2	2	2	2	2	5	2	2	4	3	2	4
200m. 1st CZ	-	-	49/52	-	-	49/52	-	48/52	47/53	-	-	48/52	-	-	-	-	-	-	-	-	-
200m. 2nd CZ	-	-	-	-	-	-	-	-	98/98	-	-	-	-	-	-	-	-	-	-	-	-

Table 5. Predicted sonar ranges for a source at 100 m depth and projecting northward when the source is located at each of the stations indicated. A (-) indicates no CZ.

Station ID	139				138				137				136				135				134				133			
	50	200	800		50	200	800		50	200	800		50	200	800		50	200	800		50	200	800		50	200	800	
Frequency (Hz)																												
Receiver Depth, Sound Path	Predicted Sonar Ranges (km)																											
5m, Direct	2	2	3		2	2	3		2	2	3		2	2	3		2	2	3		2	2	3		2	2	3	4
5m, 1st CZ	-	-	40/52		-	48/51	48/51		-	-	40/52		-	-	-		-	-	-		-	-	-		-	-	-	-
5m, 2nd CZ	-	-	-		-	-	-		-	-	-		-	-	-		-	-	-		-	-		-	-	-	-	-
100m, Direct	3	4	4		3	3	3		3	4	3		3	3	3		3	4	3		3	4		3	4	3	4	4
100m, 1st CZ	48/52	47/52	47/54		47/52	49/52	47/52		47/52	47/52	47/52		48/52	47/51	48/52		48/52	49/50	48/51		48/52	48/52		48/52	48/52	48/52	48/52	48/51
100m, 2nd CZ	96/98	96/100	96/99		97/100	97/98	98/98		97/100	97/98	-		97/100	-	97/99		98/100	96/99	96/99		97/100	98/100		97/100	97/99	97/99	96/100	96/100
200m, Direct	4	4	6		4	4	5		4	5	6		4	4	4		4	4	4		4	4		4	4	4	4	4
200m, 1st CZ	-	-	40/54		40/53	47/53	48/53		45/54	46/53	47/54		46/52	47/52	46/53		46/53	47/52	47/52		47/52	47/52		47/52	47/52	47/52	47/52	47/52
200m, 2nd CZ	-	-	95/100		-	97/101	97/100		98/99	96/100	98/100		97/100	96/98	96/98		96/98	100/100	96/98		96/98	96/98		96/100	96/98	96/100	96/100	96/100

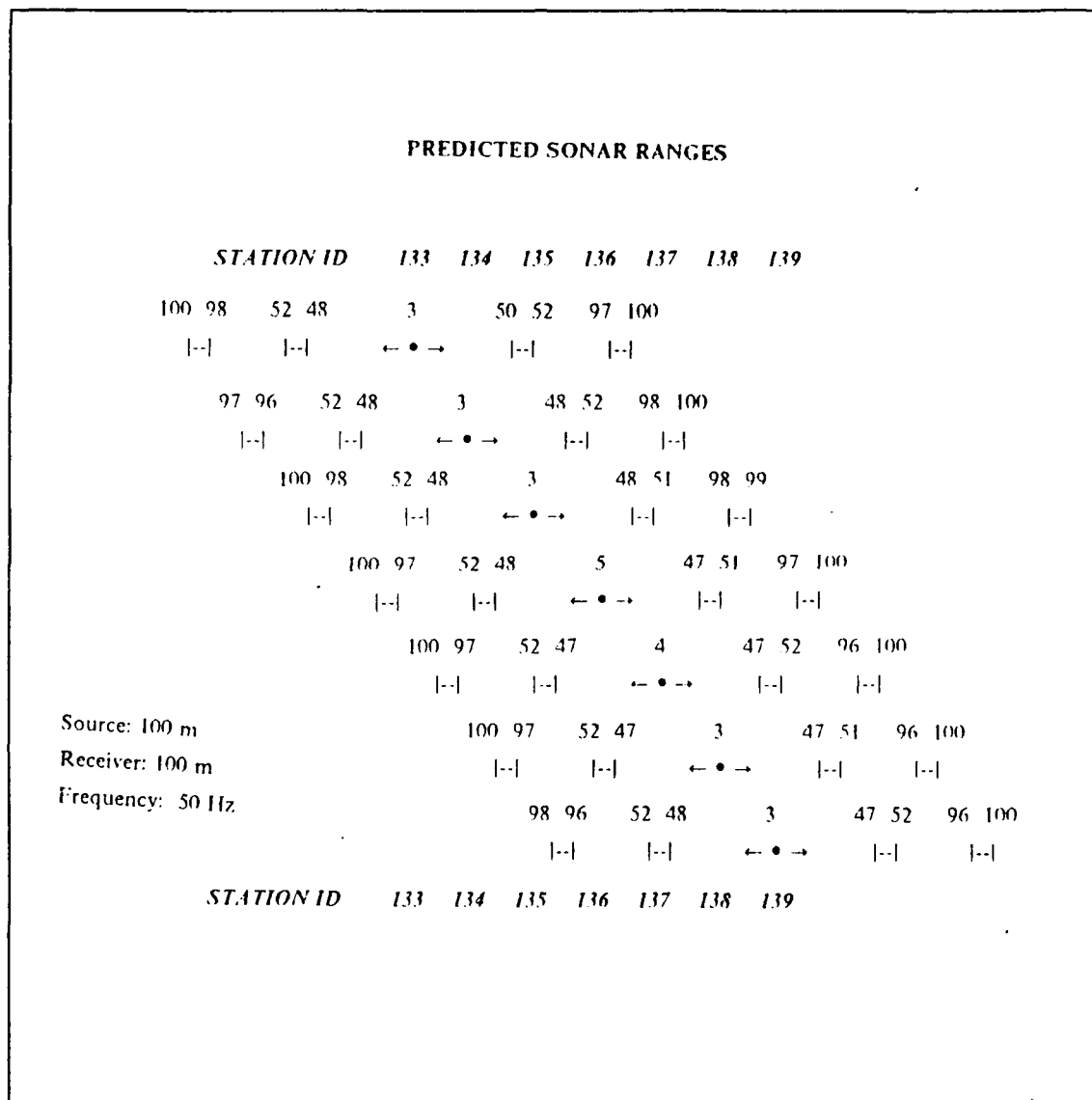


Figure 16. A geographical representation of the predicted sonar ranges: The source is at 100 m, the receiver is at 100 m and the source frequency is 50 Hz. Arrows indicate the direct path range projected north or south from the source. The source position is identified by a solid circle. Bracketed values (|--|) indicate the distance to the inner and outer edge of the convergence zone (when present). Direct path and CZ ranges (km) are indicated above each graphical symbol.

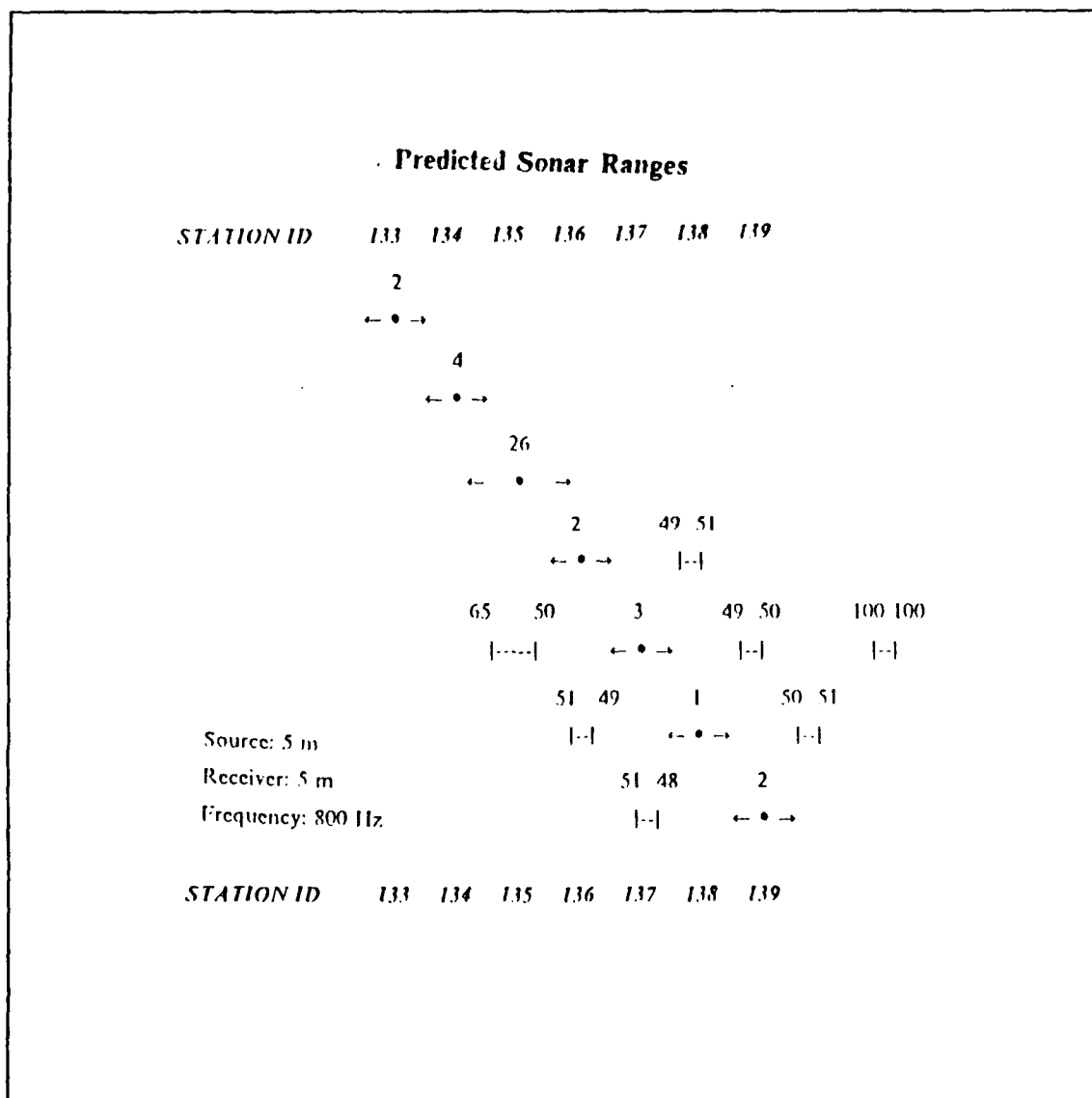


Figure 17. A geographical representation of the predicted sonar ranges: The source is at 5 m, the receiver is at 5 m and the source frequency is 800 Hz. Arrows indicate the direct path range projected north or south from the source. The source position is identified by a solid circle. Bracketed values (|--|) indicate the distance to the inner and outer edge of the convergence zone (when present). Direct path and CZ ranges (km) are indicated above each graphical symbol.

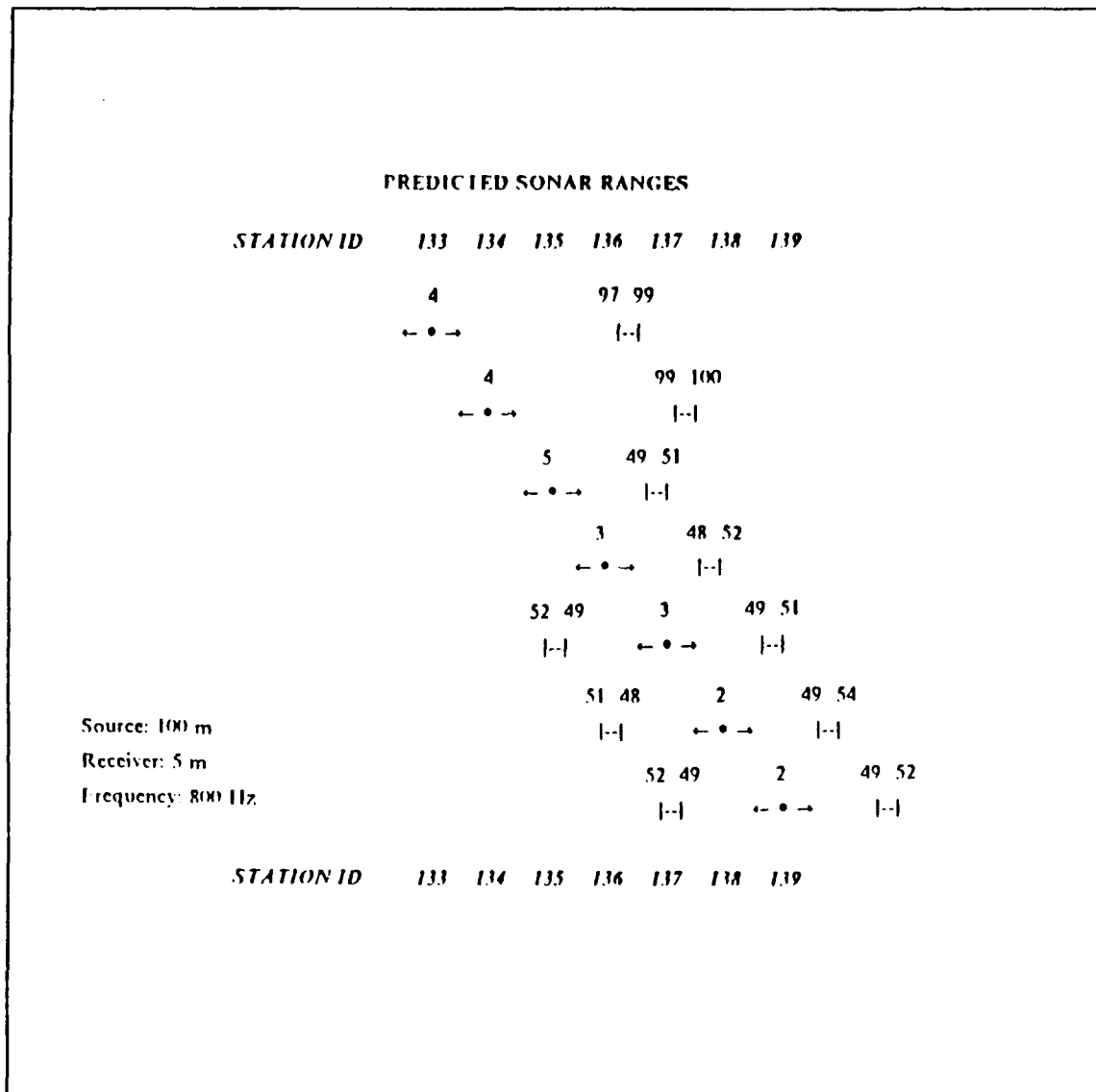


Figure 18. A geographical representation of the predicted sonar ranges: The source is at 100 m, the receiver is at 5 m and the source frequency is 800 Hz. Arrows indicate the direct path range projected north or south from the source. The source position is identified by a solid circle. Bracketed values (|--|) indicate the distance to the inner and outer edge of the convergence zone (when present). Direct path and CZ ranges (km) are indicated above each graphical symbol.

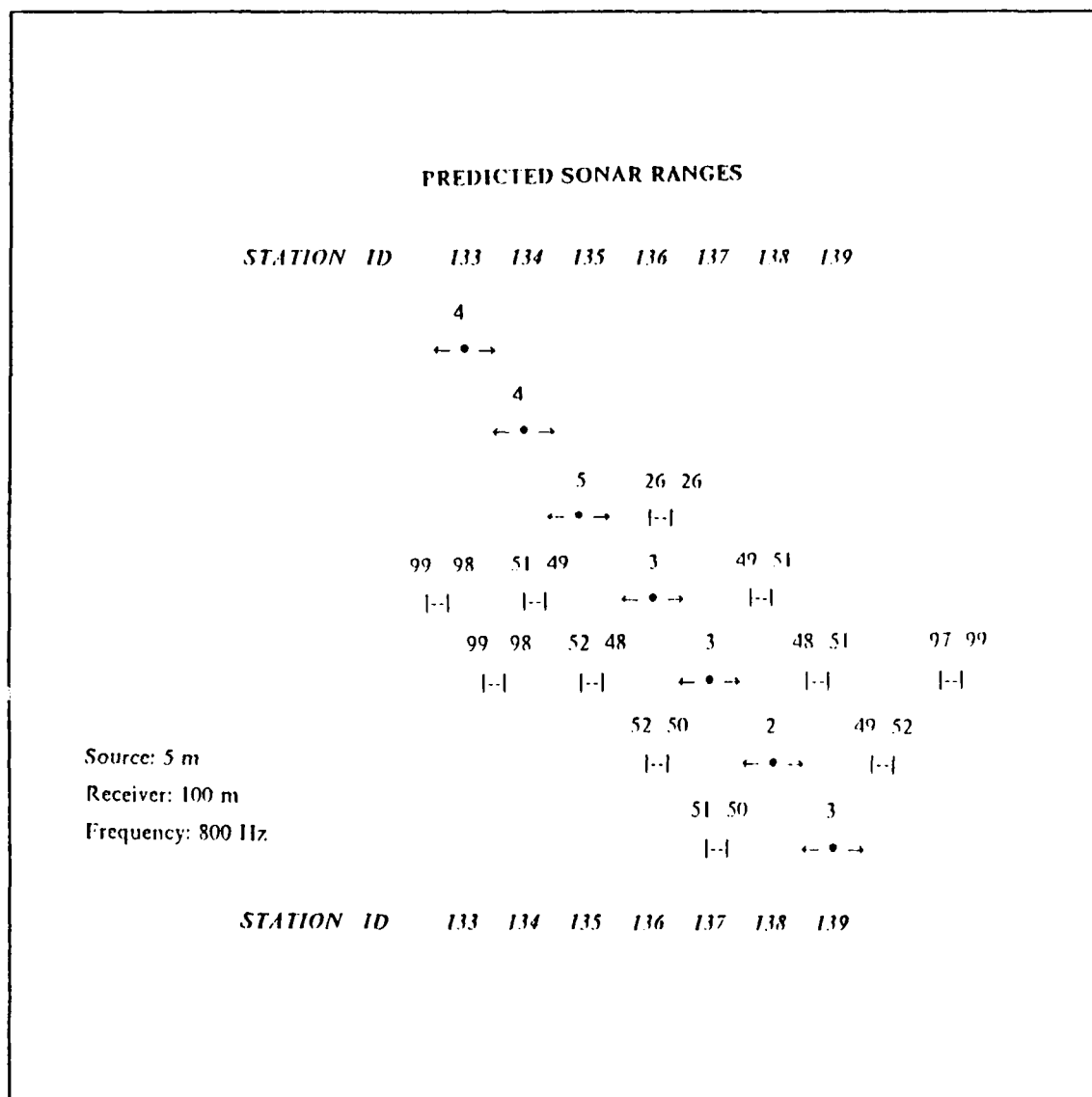


Figure 19. A geographical representation of the predicted sonar ranges: The source is at 5 m, the receiver is at 100 m and the source frequency is 800 Hz. Arrows indicate the direct path range projected north or south from the source. The source position is identified by a solid circle. Bracketed values (|--|) indicate the distance to the inner and outer edge of the convergence zone (when present). Direct path and CZ ranges (km) are indicated above each graphical symbol.

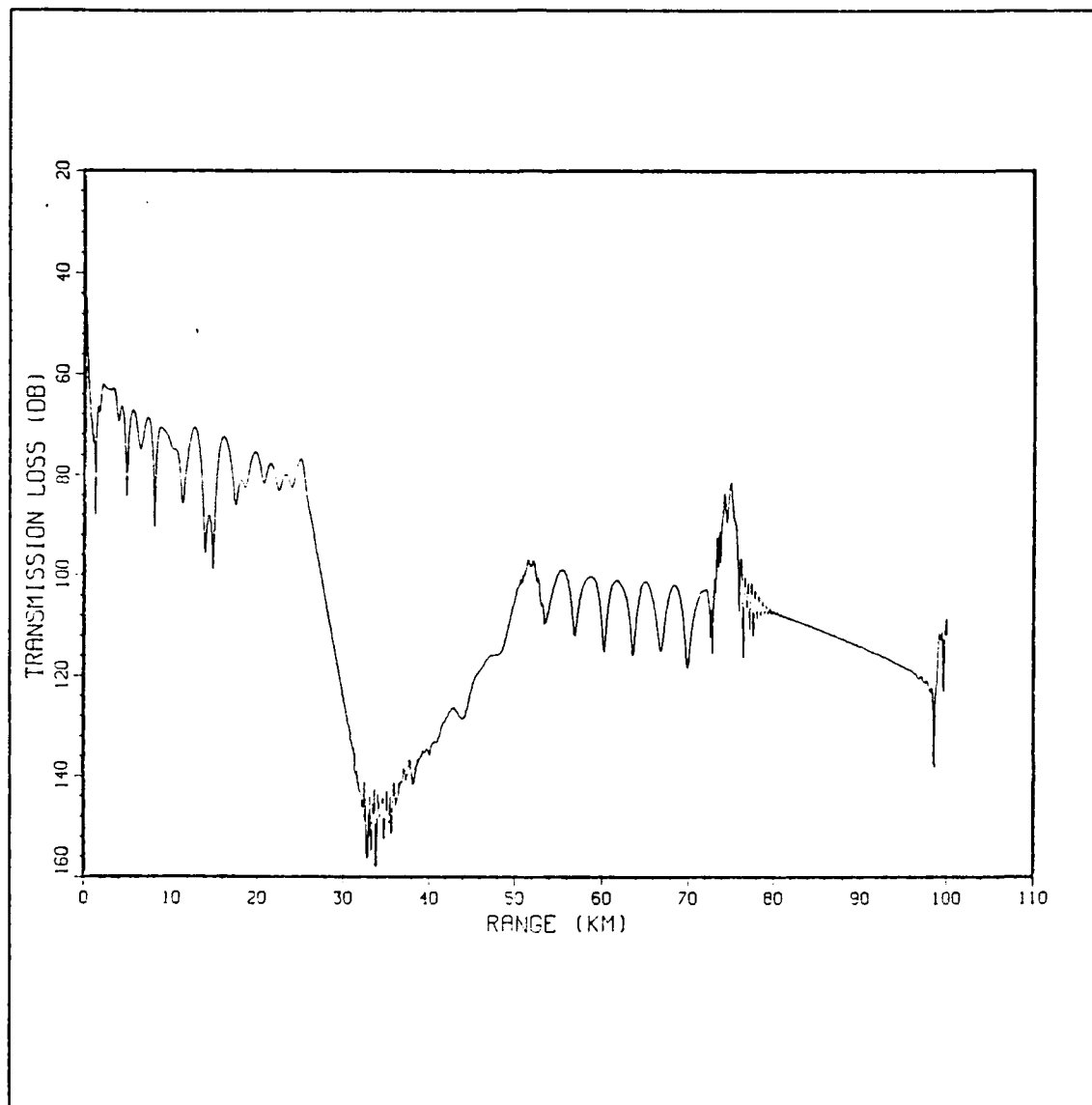


Figure 20. The PE Acoustic Model run from station 135 southward to station 139: The source depth was 5 m, the receiver depth was 5 m, and the source frequency was 800 Hz. The sharp increase in transmission loss at 26 km indicated the abrupt change in acoustic conditions at the transition between the SSP at station 135 (with its surface duct) and the SSP at station 136.

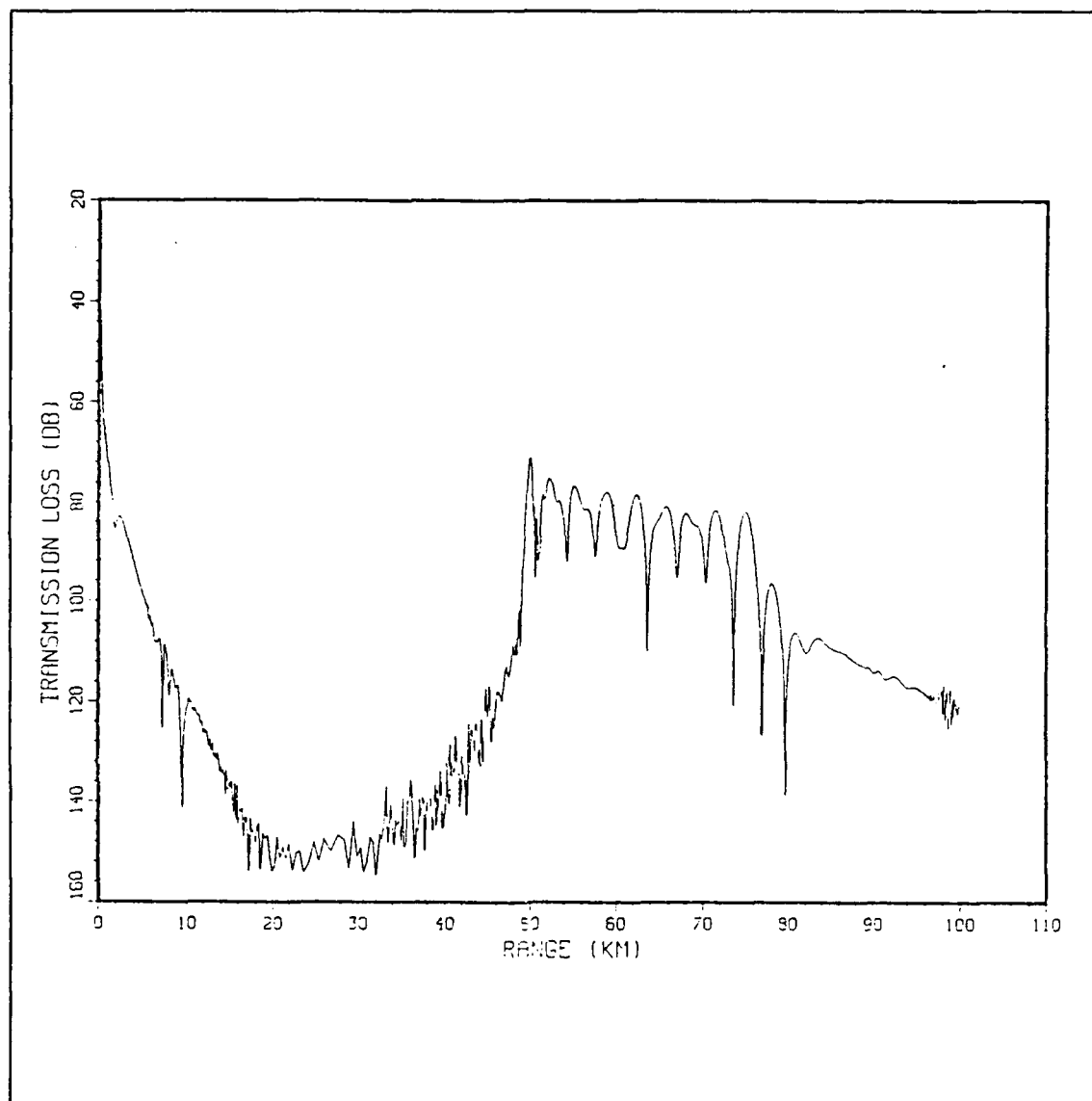


Figure 21. The PE Acoustic Model run from station 137 to station 133: The source depth was 5 m, the receiver depth was 5 m, and the source frequency was 800 Hz. The extended first convergence zone was probably due to the trapping at the surface of the first convergence signal by the surface duct at station 135.

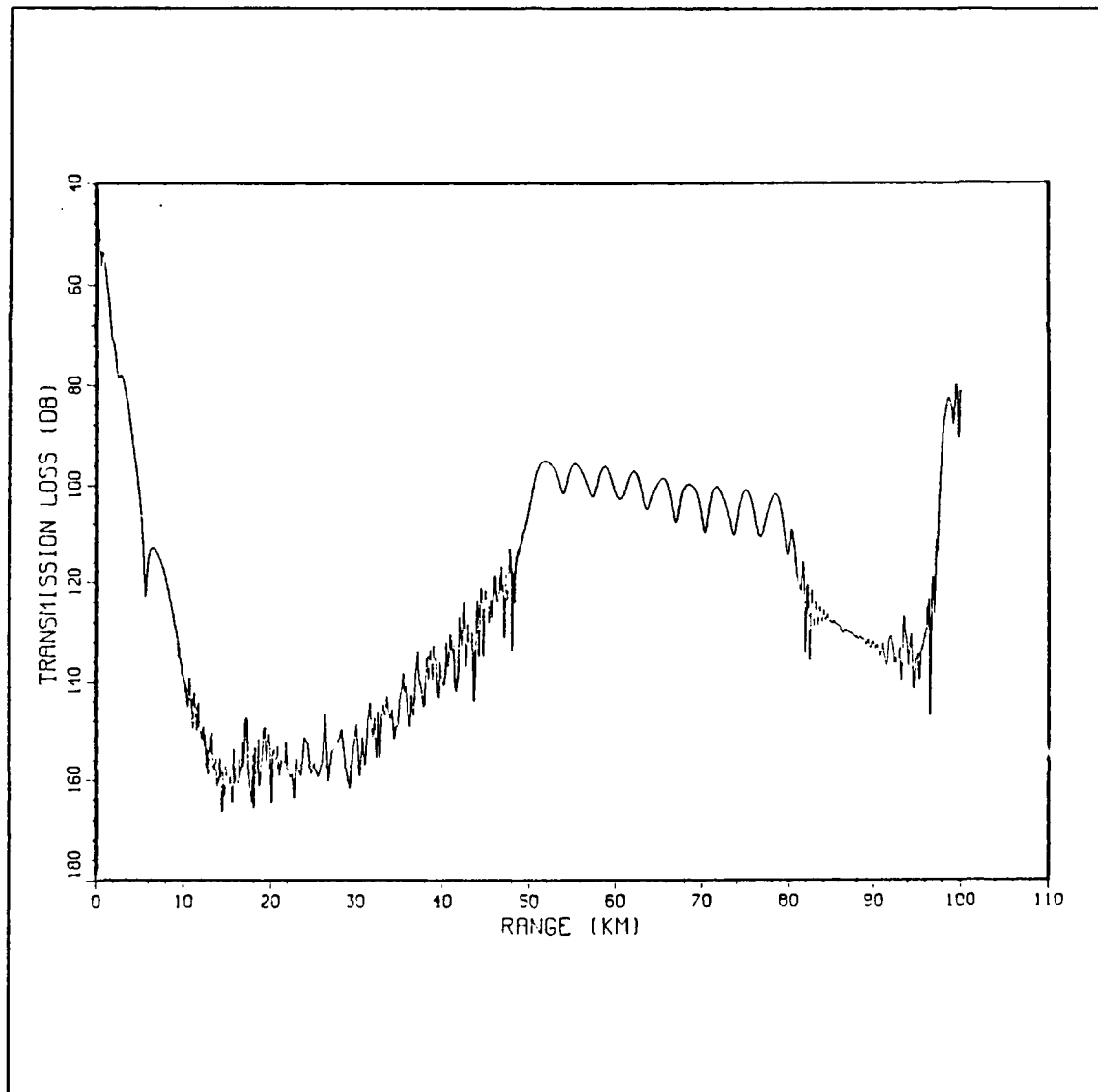


Figure 22. The PE Acoustic Model run from station 133 to station 139: The source depth was 100 m, the receiver depth was 5 m, and the source frequency was 800 Hz. The lack of a convergence zone at 50 km (while one is present at 100 km) was probably due a range dependent contraction of the depth span of the convergence rays in the vicinity of station 135 due to increased surface temperatures. The subsequent expansion of the depth span of the convergence rays in the vicinity of station 137 due to decreased surface temperatures promoted the convergence zone at 100 km.

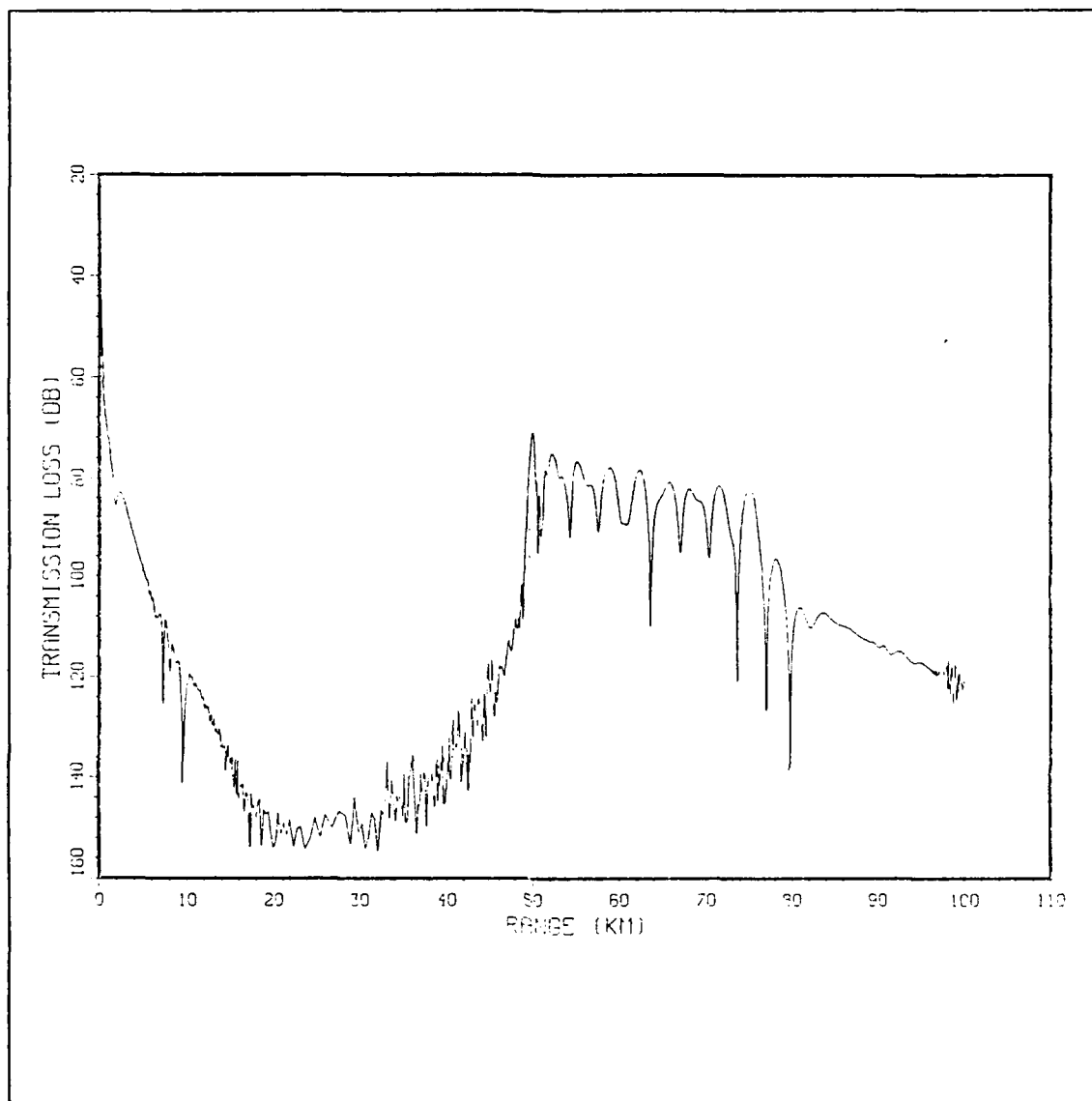


Figure 23. The PE Acoustic Model run from station 137 to station 133: The source depth was 100 m, the receiver depth was 5 m, and the source frequency was 800 Hz. The trapping of the converged signal in the surface duct in the vicinity of station 135 was apparent.

IV. DISCUSSION

A. OCEANOGRAPHY

Interest in the eastern boundary regions, and more specifically offshore cold filaments, has been greatly stimulated by the recurring appearance of these features in satellite imagery. The following is a discussion of satellite imagery which demonstrates the occurrence and dimensions of cold water filaments in eastern boundary regions around the world. The imagery used includes both sea surface temperature from the AVHRR sensor and ocean color from the CZCS. Strong gradients in ocean color which indicate high chlorophyll concentrations associated with the increased biological productivity in these nutrient rich, cool waters are plainly visible in the CZCS imagery. Although the CZCS boundaries of the cool filaments do not match the AVHRR boundaries exactly (Nykjaer et al., 1986), CZCS imagery can still be used to indicate the general size, shape, and location of the cold filaments. This is demonstrated by comparing two simultaneous AVHRR and CZCS images of a single filament (Figures 24 and 25, Nykjaer et al., 1986). These images were selected to show the chlorophyll pigment concentration and the sea-surface temperature for 2 July 1985. They were made pursuant to a study of the relationship between sea surface temperature and phytoplankton pigment concentrations in cold water filaments off the coast of Northwest Africa (Nykjaer et al., 1986). Both images revealed a filament type structure (Figures 24 and 25) with a length of approximately 200 km, a width of about 30 km, rooted near $27^{\circ} 30' \text{ N}$, $013^{\circ} 00' \text{ W}$. The AVHRR image showed a horizontal temperature gradient of about $2.5^{\circ}\text{C}/25 \text{ km}$, which was similar in strength to the filament observed off California.

Oceanographic data from the coast of South Africa indicate that cold water filaments also occur repeatedly in this region near coastal topographic features. The num-

ber, size, and location of filaments detected by satellite imagery off the coast of South Africa during February 1984 (Figure 26) show this phenomenon. During the sample interval, clouds obscured the sea surface for more than two thirds of the time (Lutjeharms et al., 1988) hence this composite was based on the remaining clear days. Each line in the figure represents the axis of a filament. The filaments in this South African region were found to extend from 50 to 600 km seaward of the main upwelling fronts. A separate study using *in-situ* oceanographic data off Namibia, Southwest Africa (Shillington et al., 1989), showed gradients of 3.7°C 25 km near a cold filament about 2 weeks old. These gradients are somewhat stronger than those observed in this study off California.

Cold filaments have also been studied off the west coast of Portugal where long filaments of cold upwelled waters extend zonally offshore for a few hundred kilometers (Fiuza, 1983). Ongoing studies of multi-year sequences of satellite imagery indicate that such filaments tend to recur near the same places off the coast of Portugal (Fiuza and Sousa, 1988). One feature off Portugal (Figure 27) is approximately 150 km long. Similar cold filaments off Portugal have been found, by *in situ* measurements, to have temperature gradients of about 3°C 25 km (Fiuza and Sousa, 1988).

The California current system is the most intensely studied eastern boundary region in the world. It contains various poleward and equatorward, surface and subsurface, mean and seasonal flows (Hickey, 1979). The basic state consists of an equatorward mean flow driven by wind stress over the eastern North Pacific (Niiler and Brink, 1989). Coastal upwelling, driven by equatorward wind stress and the resulting offshore Ekman transport of surface waters (Huyer et al., 1987), is a seasonal feature, occurring between the months of May and October. This upwelling creates an upwelling front and a geostrophically balanced equatorward current jet flows along the front (Brink, 1983). Recent observations (CTZ group, 1988) suggests that this equatorward jet begins to

meander at some point, which allows the cold water to extend far offshore within the meander (Figure 28) in the form of a cold filament. As it travels farther offshore the water in the jet is warmed by insolation and mixing with warmer surrounding waters and gradually loses its identity. Additionally, there is some evidence of subsidence of the cold salty water along the upwelling front as the filament moves offshore (The CTZ Group, 1988). The satellite observation of cold filaments of similar scale in other eastern boundary regions suggests that equatorward wind stress, coastal upwelling, and inshore coastal geometry and bottom topography are all essential ingredients necessary for the their formation. More detailed dynamical comparisons must await better *in-situ* data sets from other parts of the world.

B. ACOUSTICS

1. The Nature of the Front

The overwhelming influence of temperature on the speed of sound makes the acoustic front strongly dependent on horizontal variations in temperature. The temperature cross section (Figure 4) indicates a surface temperature gradient of $1.6^{\circ}\text{C}/25\text{ km}$ between the cold filament in this study and the warmer water to the north. This probably represents an underestimate since the 25 km station spacing was not adequate to resolve the maximum gradients. Other studies using a continuous-sampling thermosalinograph (Snow, 1988) have demonstrated maximum gradients of $1.6^{\circ}\text{C}/\text{km}^{-1}$. The vertical extent of the thermal front in Figure 4 was relatively shallow, less than 300 m.

This acoustic front can be compared to other well-studied acoustic fronts. The Gulf Stream front, a strong acoustic front, has a temperature gradient of $4^{\circ}\text{C}/25\text{ km}$ and extends to a depth of 800 m (Richardson, 1983). Warm core eddies from the Gulf Stream provide somewhat weaker and shallower acoustic fronts which typically have gradients of $2.5^{\circ}\text{C}/25\text{ km}$ and a vertical extent of 600 m (Richardson, 1983). Features

more closely resembling those of the cold filament of our study were observed near the ice edge eddies in the marginal ice zone studied by Mellberg et al., (1987). Mellberg et al. found a horizontal gradient in sound speed of 18 m s^{-1} across these eddies, which was very close to the 15 m s^{-1} gradient which existed across the cold filament off Point Arena. Using a parabolic equation model, Mellberg et al. found that transmission losses across the features were also similar. Mellberg et al. reported a change of 10 dB across the ice edge eddy. In this study, calculations of the transmission loss with source and receiver at 5 m depth and a source frequency of 800 Hz, from station 134 to 138, produced a propagation loss across the cold filament of 8 dB. This comparison is not complete because the input of initial conditions in the models for the two situations are not consistent. As they were examining a deeper structure, Mellberg et al.'s source and receiver were at 300 m depth, local bottom conditions were included and they identified the SOFAR channel as an important transmission path. The comparison is sufficient to show, however, that the two acoustic fronts appear similar to an order of magnitude. Mellberg et al. also found that the 50 Hz signal suffered greater attenuation than 1 kHz in range-dependent simulations. The range dependent anomalies across the cold filament of this study also displayed a frequency dependence, with the 800 Hz signal attenuated less across the northern margin of the filament (station 135) than the 50 or 200 Hz signals. This appears to be the result of the structure of the SSP at station 135 which provides a strong surface duct and a mixed layer depth of 71 m. The cutoff frequency calculated for this mixed layer depth is 335 Hz, indicating that neither 50 nor 200 Hz would be completely trapped in the surface duct while 800 Hz would be. This explains the lower losses sustained by the 800 Hz signal in the surface duct in the vicinity of station 135. Mellberg et al.'s lower losses at 1000 Hz when compared to 50 Hz are explained by reduced downward refraction and reduced surface decoupling loss at 1 kHz.

This resulted in the loss of the SOFAR channel as a transmission path for the 50 Hz signal while retaining it for the 1 kHz signal (Mellberg et al., 1987).

2. The Effects of the Acoustic Front

The variations in the predicted sonar ranges computed in this study could be separated into three classifications: Those not related to the acoustic front, those related to the acoustic front but not range dependent and those related to the acoustic front and range dependent.

1. Variations not related to the acoustic front. These included the variations which were the result of different frequencies or source and receiver depth combinations.
2. Variations related to the front but not range dependent. These were the result of variation in the acoustic environment near the source. These effects could be predicted by assuming that a horizontally homogeneous environment surrounded the source and included the influence of the mixed layer depth and the critical depth. Several examples of this are discussed below. The variations of mixed layer depth were not extreme enough to cause much change in the direct path surface duct ranges but they did determine which frequencies carried the direct path signal.

The most significant non-range dependent effects were those due to the change in critical depth brought about by changes in the surface sound speed due to variations in sea surface temperature (SST). These variations in critical depth were the primary cause of non-range dependent variability. The cumulative effect of relatively gradual changes of sea surface temperature in the horizontal was responsible for directing the deep propagation of sound to either permit or deny convergence zone transmission. Across this filament there was a spatial organization of those SSPs which allowed CZ transmission and those which did not. To the north of the filament high sound speed close to the surface prevented convergence zone transmission for a shallow (5 m) source while SSPs in the filament and to the south permitted CZ transmission for a shallow (5 m) source.

3. Variations related to the front and range dependent. There were several range dependent anomalies which were related either to the dramatic reshaping of the SSP near the surface which occurred at the northern margin of the filament at station 135 or, to the expansion or contraction of the depth band of the convergence zone ray path which occurred with range dependent variation in SST. The extended first convergence zone from station 137 to the north (Figure 21) and the first convergence range of 99 km from station 133 to the south (Figure 22) are respective examples. They were the result of unique SSPs created by the cold filament moving into a new area of warm oceanic water, providing extended first convergence zone ranges due to surface duct trapping when projecting northward from a shallow (5 m source) at station 137 and the anomalous absence of the first convergence zone in the vicinity of station 135, coupled with the appearance of a convergence zone in the vicinity of station 137 when projecting from a deep source (100 m) located at station 133 southward towards shallow receivers at 5 m. The extent and lifetime of these unique features is unknown. In our model the station spacing gives them a width of 25 km. The along-filament extent and temporal lifetime of the layering is unknown. The horizontal extent of these features is important because the dis-

tance over which they influence the environment relates directly to the affected PSRs. For example, the surface channel created by the SSP at station 133 results in near surface direct path ranges of about 25 km. If in reality the feature was smaller, the modelled direct path range would also be smaller. Other PSRs were similarly perturbed by the passage of sound energy through a simulated 25 km thick band of water with a unique SSP. Complete correction of this sampling problem is not possible. The mechanism of these effects, as described above, was discernable from the shape of the curves in Figures 21 and 22, but the distance over which they acted was probably less than indicated.

3. The Tactical Significance of Variations in PSRs

To emphasize the importance of this variation, it is useful to create a few tactical scenarios and use the PSRs calculated to determine the acoustic advantage of various relative positions across this cold filament. For all scenarios we will consider a surface ship and a submarine, each with an FOM of 80 dB and each listening for an 800 Hz signal. The surface ship as a source is constrained to the surface but can optionally lower a hydrophone to listen at 100 m. The submarine is constrained to operate and listen at 100 m.

The first scenario (Figure 29) puts the surface ship at station 134, listening at 100 m, with the submarine at station 136. In these positions, the surface ship's direct path signal can be detected at 4 km and there are no convergence zone paths. The submarine's signal, however, does produce CZ ranges allowing initial detection to occur in the second CZ at 99 km with another convergence zone at 52 km. The direct path signal can be detected by the surface ship at 4 km. The acoustic advantage in this scenario goes to the surface ship.

Next we place the surface ship at station 137, again listening at 100 m, moving the submarine to station 135 (Figure 30). The surface ship's signal can be heard via direct path to 4 km, with convergence zones at 51 and 99 km. The submarine's signal is now detectable at 4 km direct path, with convergence zones at 52 and 100 km. Both have essentially equal acoustic capabilities. Neither vessel has an acoustic advantage.

The final scenario places both the surface ship and the submarine near station 135 (Figure 31). The direct path signal of the surface ship extends to 26 km. The submarine can be detected via direct path to 4 km. There are no convergence zone ranges listed because the distance between the adversaries is less than the range to the first convergence zone. In this case the submarine has the acoustic advantage (the degree of the advantage is not accurately described by the surface ship's direct path range of 26 km for reasons stated earlier).

The significance of these scenarios is that this cold water filament produces an acoustic front sufficient to cause a change in acoustic advantage based on relative position with respect to the front. For this cold water filament a surface ship steaming offshore would be far less detectable if it stayed to the north of the cold zone, rather than transversing within it.

4. Applicability to Other Eastern Boundary Regions

Substantial variation in predicted PSRs occurred across this filament in the California Current System. This filament has a greater surface temperature change across it (5°C) than other filaments observed (based on satellite SST) in other parts of the world. This calls to question the general applicability of the results. Perhaps the cold filaments in other regions do not present enough of a temperature gradient to produce a substantial variation in sonar ranges. A review of our results indicates that not much of a temperature difference is needed. The sea surface temperature differences between station 134 and 135 was less than $1^{\circ}\text{C}/25\text{ km}$, yet there was a substantial increase in predicted sonar range at station 135 because of the structure of the shallow SSP which occurred at the margin of the filament. A change in sea surface temperature of $1^{\circ}\text{C}/25\text{ km}$ at the margin is commonly observed for other filaments measured by AVHRR imagery, but their vertical structure and degree of interleaving is largely unknown.

The shoaling of the critical depth which permitted convergence zone transmission from near-surface sources was a function only of temperature at the surface. A change in surface temperature of 2.2°C between stations 134 and 136 made the difference between CZ reception at the surface at 136 and no CZ at the surface at station 134. A temperature gradient of $1.1^{\circ}\text{C}/25\text{ km}$ was enough to create a substantial difference. The cold filaments in other regions discussed above (Figures 24 and 27) have temperature gradients which exceeded $1.1^{\circ}\text{C}/25\text{ km}$, and could provide similar PSR variations.



Figure 24. AVHRR image of a cold filament off NW Africa on 2 July 1985: The black crosses indicate 1° squares with north toward the top. Shades of grey are indicative of sea surface temperature, a scale in °C is provided across the top (From Nykjaer et al., 1986). The arrow indicates location of coldest water in the filament.



Figure 25. CZCS image of the region in Figure 24 on 2 July 1985: The cold filament of Figure 24 is plainly visible as a chlorophyll maximum in this image (From Nukjaer et al.,1986).

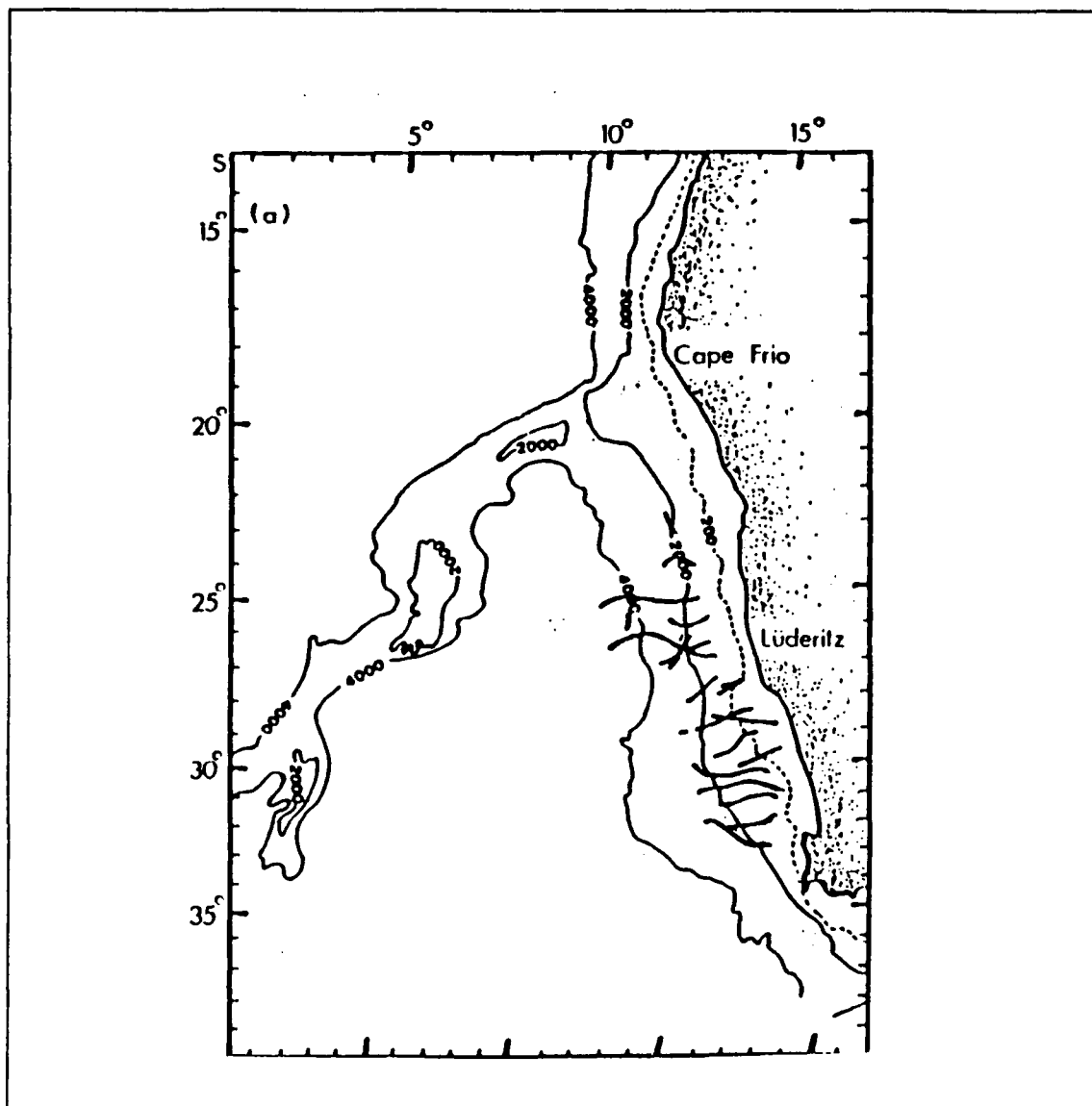


Figure 26. All cold filaments which occurred off South Africa in February 1984 from satellite AVHRR data: The position and orientation of each filament observed is indicated by a solid line. The observed cold filaments were between 50 km and 600 km in length (From Lutejeharms et al., 1988).



Figure 27. AVHRR image of a cold filaments off the coast of Portugal on 21 AUG 1979.: The arrow indicates the best defined filament. This cold filament extended approximately 150 km offshore. The coldest water is white and the darker shades are warm. The Straits of Gibraltar are at the top (From Fiuza, 1985).

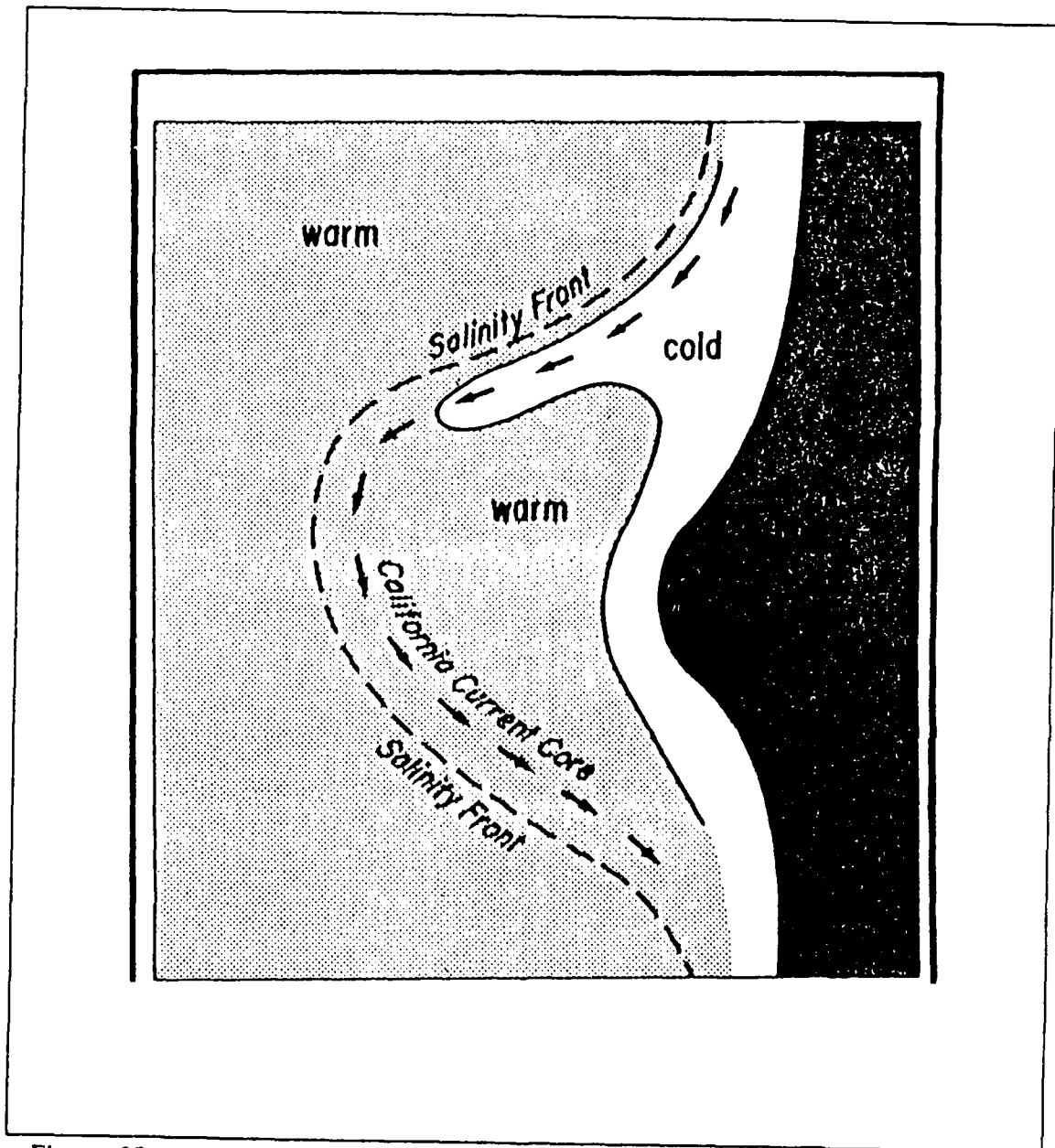


Figure 28. A schematic diagram of an offshore cold filament. (From The CTZ Group, 1988)

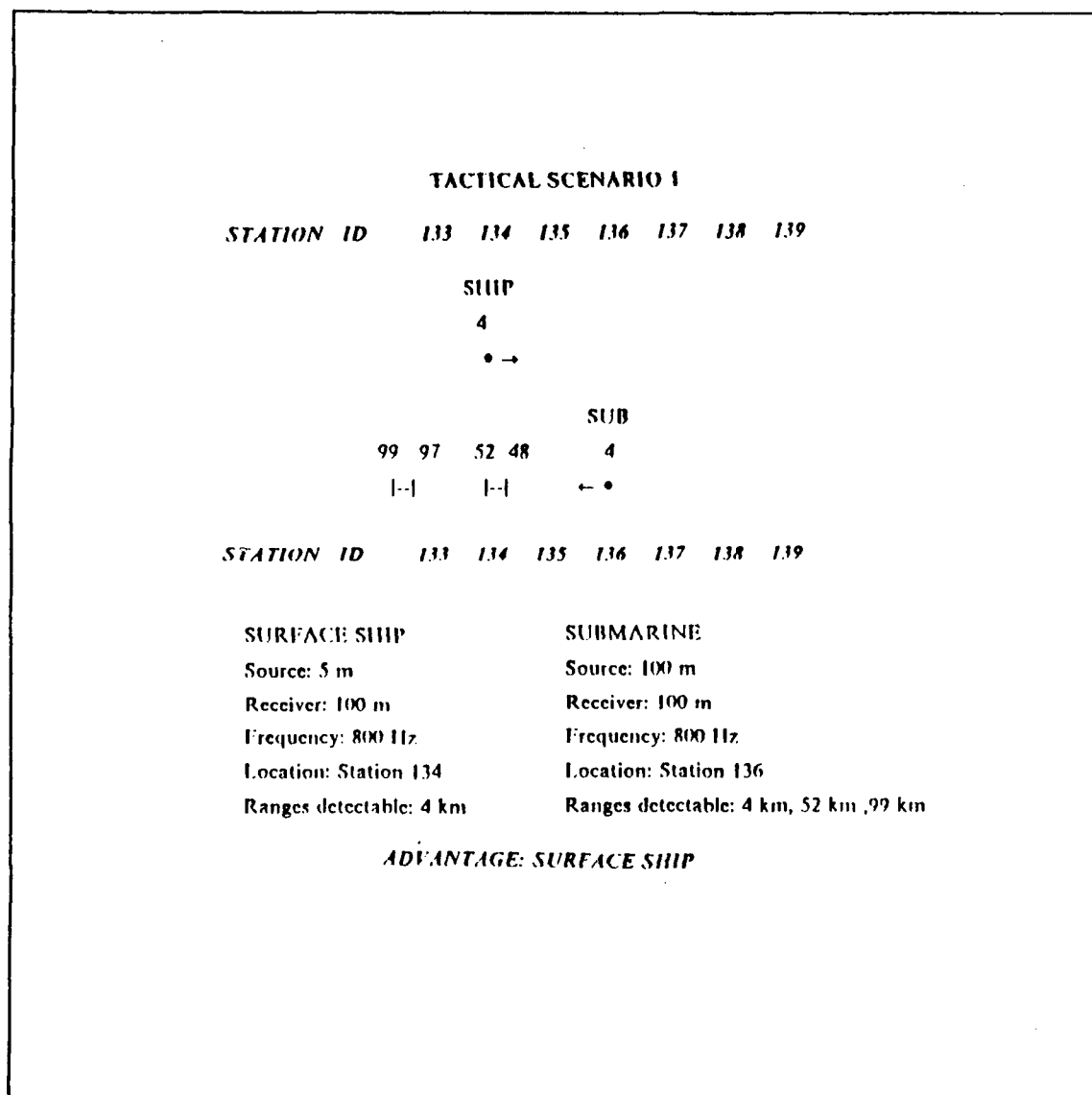


Figure 29. Tactical Scenario #1: A surface ship at station 134 at 5 m with a hydrophone at 100m and a submarine at station 136 at 100 m. Arrows indicate the direct path range projected from the source towards the adversary. Source position is identified by solid circle. Bracketed values (|--|) indicate the distance (km) to the inner and outer edge of the convergence zone (when present).

TACTICAL SCENARIO 2

STATION ID 133 134 135 136 137 138 139

SHIP

100 99 51 49 4
 |--| |--| ← •

SUB

4 48 53 98 100
 • → |--| |--|

STATION ID 133 134 135 136 137 138 139

SURFACE SHIP

Source: 5 m
 Receiver: 100 m
 Frequency: 800 Hz
 Location: Station 137
 Ranges detectable: 4 km, 51 km, 100 km

SUBMARINE

Source: 100 m
 Receiver: 100 m
 Frequency: 800 Hz
 Location: Station 135
 Ranges detectable: 4 km, 53 km, 100 km

NO ACOUSTIC ADVANTAGE

Figure 30. Tactical Scenario #2: A surface ship at station 137 at 5 m with a hydrophone at 100m and a submarine at station 136 at 100 m. Arrows indicate the direct path range projected from the source towards the adversary. Source position is identified by solid circle. Bracketed values (|--|) indicate the distance (km) to the inner and outer edge of the convergence zone (when present).

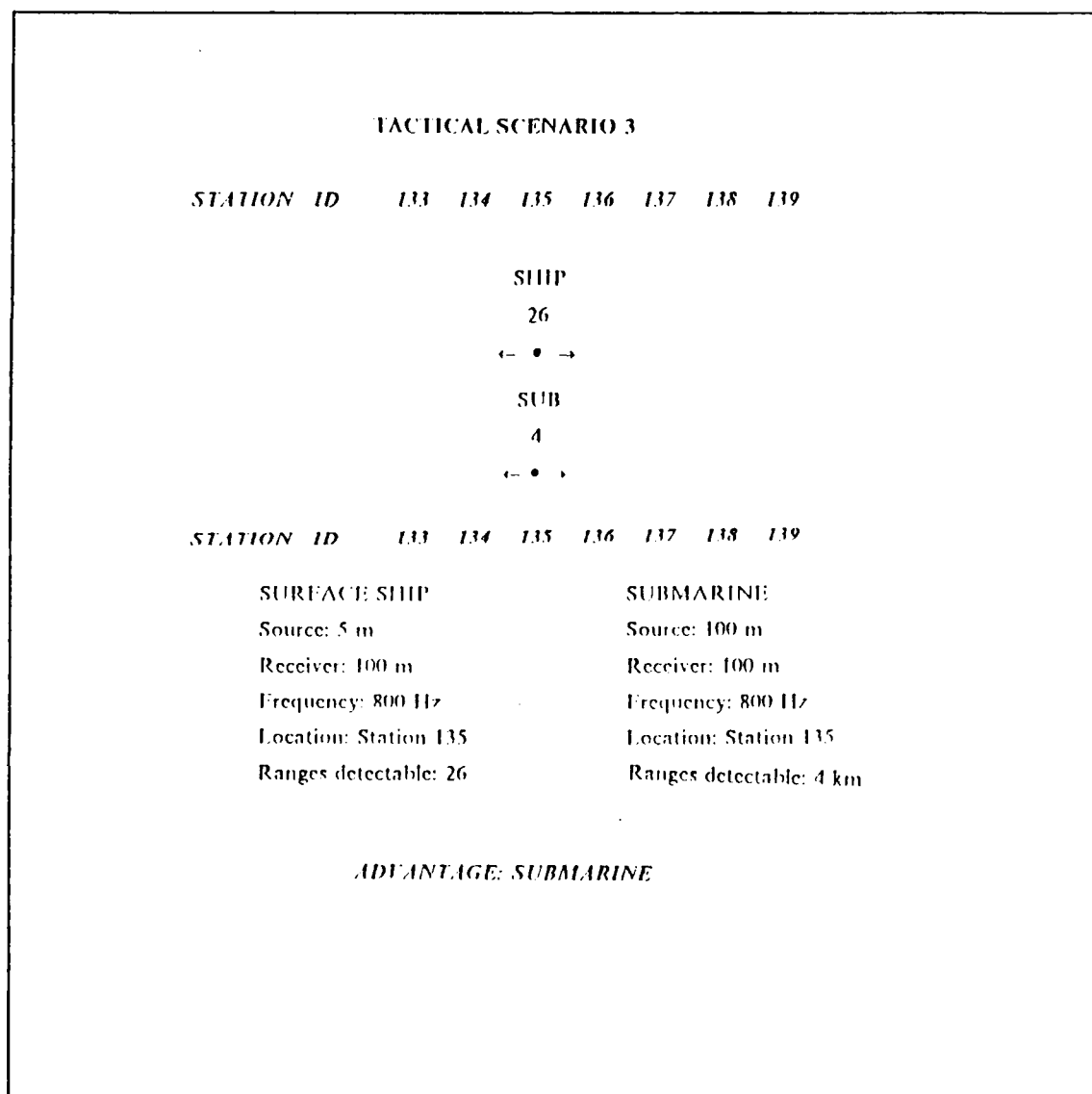


Figure 31. Tactical Scenario #3: A surface ship at station 135 at 5 m with a hydrophone at 100m and a submarine at station 135 at 100 m. Arrows indicate the direct path range (km) projected from the source towards the adversary. Source position is identified by solid circle. Since the ship and sub are within 25 km of each other, CZ ranges are not relevant.

V. CONCLUSION

Cold filaments recur off prominent coastal features in strategically important coastal areas in oceanic eastern boundary regions around the world. They are detectable by satellite using either infrared or color imagery from either the AVHRR or CZCS instruments.

The cold filament investigated in this study presented an acoustic front in the upper 300 m of the water column which was sufficient to change the acoustic advantage between two adversaries operating in that depth band depending on their positions relative to each other and to the acoustic front.

The three acoustic mechanisms responsible for the filament-related variation in PSRs were:

1. The inception of convergence zone transmission at a location caused by a decrease in surface temperature.
2. The extension of ranges by surface ducting which was the result of the overriding of cold filament water over the warmer water at the margin of the filaments.
3. The expansion and contraction of the depth band of the convergence zone ray path, which acted to provide or deny convergence zone transmissions to shallow sensors.

None of these mechanisms required strong horizontal temperature gradients. Although the cold filament of this study contained a temperature difference of 5 °C from the coldest water near the center of the filament to the warmer water outside, much smaller differences were responsible for the variations in PSRs which occurred between stations. Temperature differences of no more than 1 °C/25 km were sufficient to determine whether or not CZ transmission occurred. Differences of less than 1 °C existed between the stations on either side of the margin of the filament. All of the filaments presented as examples in this paper had such gradients. Similar mechanisms depending on similar temperature gradients would be valid in the area of cold filaments wherever they occurred. This implies that similar acoustic fronts could be presented by cold filaments

where ever they are detected by satellite imagery, and that these cold filaments present acoustic fronts at shallow depths which are sufficient to effect a tactical advantage.

LIST OF REFERENCES

- Batteen, M. L., R. L. Haney, T. A. Tielking, P. G. Renaud, 1989: A Numerical Study of Wind Forcing of Eddies and Jets in the California Current System. *Journal of Marine Research*, 47, 493-523.
- Brink, K. H., 1983: The Near Surface Dynamics of Coastal Upwelling. *Progress in Oceanography*, 12, 223-257.
- Brink, K. H., 1985: Some Aspects of Physical Processes in Coastal Upwelling. *International Symposium on Upwelling off West Africa*, 1, 5-14. Ins. Inv. Pesq. Barcelona.
- Brink, K. H., 1987: Upwelling Fronts: Implications and Unknowns. *South African Journal of Marine Science*, 5, 3-9.
- Brink, K. H., E. O. Hartwig, 1985: *Office of Naval Research Coastal Transition Zone Workshop Report*, Naval Postgraduate School, Monterey, California, May 6-8, 1985.
- Coppens, A. B., 1982: *An Introduction to the Parabolic Equation for Acoustic Propagation*. Naval Postgraduate School, Monterey, Ca.
- Colborn, J.G., 1975: The thermal structure of the Indian Ocean. International Indian Ocean Expedition Monograph No. 2. Naval Ocean Research and Development Activity, NSTL Station, MS.
- Crepon, M., C. Richez, and M. Chartier, 1984. The Effect of Coastline Geometry on Upwellings. *Journal Physical Oceanography*, 14, 1365- 1382.
- CTZ Group, 1988: The Coastal Transition Zone Program. *EOS*. Transactions of the American Geophysical Union, July 5, 1988, 698-707.
- Daggett F., 1989: A Study of the Velocity near a Cold Filament from ADCP and CTD Measurements. M. S. Thesis, Naval Postgraduate School, Monterey California.
- Davis, R. E., 1985: Observations of Coastal Surface Currents During CODE. The Method and Descriptive View. *Journal of Geophysical Research*, 90, C3,4741-4755.
- Flament, P., L. Armi and L. Washburn, 1985: The Evolving Structure of an Upwelling Filament. *Journal of Geophysical Research*, 90, 11, 765-778.
- Fiuza, A. F. G., 1985: *Proceedings of the First International Symposium on the Iberian Coastal Upwelling*. Lisbon, Portugal
- Fiuza, A. F. G. and F. M. Souza, 1989: Preliminary Results of a CTD Survey in the Coastal Transition Zone off Portugal During 1 - 9 September 1988. *Coastal Transition Zone Newsletter*, 4, 1, 2-10.

- Fofonoff, N. P., and R. C. Millard, Jr., 1985: Algorithms for Computation of Fundamental Properties of Seawater. *UNESCO Technical Journal*.
- Hickey, B. M., 1979: The California Current System: Hypotheses and Facts. *Progress in Oceanography*, 8, 191-279.
- Huyer, A., 1983: Coastal Upwelling in the California Current System. *Progress in Oceanography*, 12, 259-284.
- Huyer, A. and P. M. Kosro, 1987: Mesoscale Surveys over the Shelf and Slope in the Upwelling Region Near Pt. Arena, California. *Progress in Oceanography*, 12, C2, 1655-1681.
- Kosro, P. M., AND A. Huyer, 1986. CTD and Velocity Surveys of Seaward Jets off Northern California, July 1981 and 1982. *Journal of Geophysical Research* 91, C6, 7680-7690.
- Ikeda, M., and W. J. Emery, 1984: Satellite Observations and Modeling of Meanders in the California Current System off Oregon and Northern California. *Journal of Physical Oceanography*, 14, 1434-1450.
- Lutjeharms, J. R. E. and P. L. Stockton, 1987: Kinematics of the Upwelling Front off Southern Africa. *The South Africa Journal of Marine Science*, 5, 35-49.
- Mellberg, L. E., and O. M. Johannessen, D. N. Connors, G. Botseas, and D. Browning, 1987: Modeled Acoustic Propagation Through an Ice Edge Eddy in the East Greenland Sea Marginal Ice Zone. *Journal of Geophysical Research*, 92, C7, 6857-6868.
- Mysak, L. A., E. R. Johnson and W. W. Hsieh, 1981: Baroclinic and Barotropic Instabilities of Coastal Currents. *Journal of Physical Oceanography*, 11, 2, 209-230.
- Narimousa, S. A., T. Maxworthy 1987: Coastal Upwelling on a Sloping Bottom : The Formation of Plumes, Jets and Pinched-off Cyclones. *Journal of Fluid Mechanics*, 176, 169-190.
- Niiler, P. P., 1969: On the Ekman Divergence in an Oceanic Jet. *Journal of Geophysical Research*, 74, 7048-7051.
- Nyijkjaer, L. L. Van Camp and N. Hojerslev, 1986: *Remote Sensing of the Northwest African Upwelling Area, II*, University of Copenhagen Press, Copenhagen N. Denmark.
- Reinecker, M. M., A.R. Robinson, and C. N. K. Mooers, 1987: The Evolution of Synoptic Mesoscale Features off Northern California During Summer 1984: A Description Using Data Analysis and Dynamic Model Forecast Experiments. *Journal of Physical Oceanography*, 17, 8, 1189 - 1213.
- Reinecker, M. M., C. N. K. Mooers, D. E. Hogan, and A. R. Robinson, 1985: A Cool Anomaly off Northern California: An Investigation Using IR imagery and in situ data. *Journal of Geophysical Research*, 90, C3, 4807-4818.

- Shillington, F. A., W. T. Peterson, L. Hutchings, T. A. Probyn, H. N. Waldron, and J. J. Agenbag, 1989: A Cool Upwelling Filament off Namibia, South Africa: Preliminary Measurements of Physical and Biological Features. *Coastal Transition Zone Newsletter*, 4, 1, 10-35.
- Simpson, J. J., T. D. Dickey and C. J. Koblinsky, 1984: An Offshore Eddy in the California Current System Part I: Interior Dynamics. *Progress in Oceanography*, 13, 5-49.
- Smith R. L., 1981: A Comparison of the Structure and Variability of the flow field in the Three Coastal Upwelling Regions: Oregon, Northwest Africa, and Peru. In: *Coastal Upwelling* F.A. Richards, editor, American Geophysical Union, Washington, D. C.
- Snow R. L., 1988: Sea Surface Temperature and Salinity Structure in Cold Upwelling Filaments Near Point Arena as Observed Using Continuous Underway Sampling Systems. M. S. Thesis, Naval Postgraduate School, Monterey California.

INITIAL DISTRIBUTION LIST

		No. Copies
1.	Defense Technical Information Center Cameron Station Alexandria, VA 22304-6145	2
2.	Library, Code 0142 Naval Postgraduate School Monterey, CA 93943-5002	2
3.	Chairman (Code 63Rd) Department of Meteorology Naval Postgraduate School Monterey, CA 93943-5000	1
4.	Chairman (Code 68Co) Department of Oceanography Naval Postgraduate School Monterey, CA 93943-5000	1
5.	Office of Naval Research Code 1122PO 800 North Quincy Street Arlington, VA 22217 Attn: Dr. Tom Kinder	1
6.	Director Naval Oceanography Division Naval Observatory 34th and Massachusetts Avenue NW Washington, DC 20390	1
7.	Commander Naval Oceanography Command Naval Oceanography Command Stennis Space Center, MS 39529-5000	1
8.	Commanding Officer Fleet Numerical Oceanography Center Monterey, CA 93943	1
9.	Commanding Officer Naval Oceanographic Office Stennis Space Center, MS 39522-5001	1
10.	Commanding Officer Naval Ocean Research and Development Activity Stennis Space Center, MS 39522-5001	1

11. Commanding Officer 1
Naval Environmental Prediction Research Facility
Monterey, CA 93943-5006
12. Chairman, Oceanography Department 1
U. S. Naval Academy
Annapolis, MD 21402
13. Office of Naval Research (Code 420) 1
Naval Ocean Research and Development Activity
800 North Quincy Street
Arlington, VA 22217
14. Professor Steve Ramp (Code 68Ra) 1
Department of Oceanography
Naval Postgraduate School
Monterey, CA 93943-5000
15. Office of Naval Research 1
Code 1122PO
800 North Quincy Street
Arlington, VA 22217
Attn: Dr. David Evans
16. Professor Robert H. Bourke (Code 68Bf) 1
Naval Postgraduate School
Monterey, CA 93943-5000